Stony Brook University

Biological Roles and Regulation of Phosphatidylinositol 3-Kinase (PI3K) Isoforms

A Dissertation Presented

by

Mohar Chattopadhyay

to

The Graduate School

in Partial Fulfillment of the

Requirements

for the Degree of

Doctor of Philosophy

in

Physiology and Biophysics

Stony Brook University

May 2010

Stony Brook University

The Graduate School

Mohar Chattopadhyay

We, the dissertation committee for the above candidate for the
Doctor of Philosophy degree, hereby recommend
acceptance of this dissertation.

Richard Z. Lin
Professor, Department of Medicine & Physiology and Biophysics

Raafat El-Maghrabi
Research Associate Professor, Department of Physiology and Biophysics

Peter R. Brink
Professor, Department of Physiology and Biophysics

Suzanne Scarlata
Professor, Department of Physiology and Biophysics

Howard Crawford
Associate Professor, Department of Pharmacological Sciences

Wei-Xing Zong
Assistant Professor, Department of Molecular Genetics and Microbiology

This dissertation is accepted by the Graduate School

Lawrence Martin
Dean of the Graduate School

Abstract of the Dissertation

Biological Roles and Regulation of Phosphatidylinositol 3-Kinase (PI3K) Isoforms

by

Mohar Chattopadhyay

Doctor of Philosophy

in

Physiology and Biophysics

Stony Brook University

2010

Class IA PI3Ks are signaling molecules that control cell survival, growth, proliferation and metabolism. Dysregulated PI3K signaling is found in patients with diseases such as diabetes and cancer. The two aims of my thesis research were (1) to determine the distinct roles of the PI3K isoforms p110α and p110β in regulating hepatic lipid and glucose metabolism and (2) to investigate the regulation of p110α and p110β by the heterotrimeric G protein $G\alpha_q$. For aim 1, mice with liver-specific gene deletion of p110α or p110β were generated. My studies found that mice lacking hepatic p110α were largely protected from high-fat diet-induced liver steatosis, whereas p110β ablation did not attenuate triglyceride accumulation in the liver. The protective effect of p110α ablation is probably due to decreased liver uptake of long chain fatty acids. High-fat diet-induced increases in mRNA and protein levels of liver fatty acid binding protein were blunted in

the p110α-null liver. On the other hand, mice lacking hepatic p110β developed glucose intolerance and hyperinsulinemia. Higher cAMP levels and increased expression of adenylyl cyclase 5 correlated with increased gluconeogenesis and glycogenolysis in $p110\beta^{-/-}$ hepatocytes. Mice with p110α-null liver did not exhibit glucose intolerance or hyperinsulinemia. Furthermore, ablation of p110α decreased insulin signaling in the liver, whereas deletion of p110β had relatively minor effects on this signaling pathway.

Aim 2 of my thesis research investigated the mechanism by which $G\alpha_q$ inhibits PI3Ks. My studies used purified recombinant proteins and fluorescence spectroscopy to demonstrate that $G\alpha_q$ directly binds to p110α and blocks Ras binding to p110α. In addition, *in vitro* PI3K activity assays revealed that $G\alpha_q$ inhibits the four PI3K enzyme complexes p110α/p85α, p110α/p85β, p110β/p85α and p110β/p85β. It was determined that $G\alpha_q$ binds to the p85-binding domain of p110α and does not appear to directly interact with the catalytic domain. Further, I found that $G\alpha_q$ can bind to free p85 in the iSH2 region independently of p110 binding.

In summary, findings from my thesis research indicate that p110α and p110β have differential effects on hepatic lipid and glucose metabolism and that activated $G\alpha_q$ can directly bind and inhibit PI3K complexes.

This dissertation is dedicated to my parents and grandparents.

Table of Contents

List of Figures

Chapter 1

Chapter 2

Chapter 3

List of Tables

Chapter 2

List of Abbreviations

1-palmitoyl-2-oleoyl phosphatidylcholine	POPC
1-palmitoyl-2-oleoyl-*sn*-glycero-3-phospho-L-serine	PS
Adenylyl cylcase 5	Adcy-5
Adenylyl cylcase 6	Adcy-6
Alanine aminotransferase	ALT
Aspartate aminotransferase	AST
Atypical protein kinase C	aPKC
Break-point cluster homology domain	BHD
Cyclic adenosine monophosphate	cAMP
Dual Energy X-Ray Absorptiometry	DEXA
Fatty acid synthase	FAS
Glucose transporter 4	GLUT4
Glucose 6-phosphatase	G6PC
Glutathione S-transferase	GST
Glycogen synthase kinase-3	GSK3
G protein-coupled receptor	GPCR
Haemagglutinin	HA
High-fat diet	HFD
Hormone-binding domain of estrogen receptor	hbER
Human embryonic kidney	HEK
Immunoprecipitation	IP

Insulin receptor substrate	IRS
Insulin-like growth factor	IGF
Large unilamellar vesicle	LUV
Liver fatty acid binding protein	L-FABP
Long chain fatty acid	LCFA
Mammalian target of rapamycin	mTOR
Peroxisome proliferator activated receptor α	PPARα
Peroxisome proliferator activated receptor γ	PPARγ
Phosphatidylinositol	PI
Phosphatidylinositol (4, 5) bisphosphate	PIP_2
Phosphatidylinositol (3, 4, 5) trisphosphate	PIP_3
Phosphatidylinositol 3-kinase	PI3K
Phosphoenolpyruvate carboxykinase	PEPCK
Phosphatase and tensin homologue deleted on chromosome ten	PTEN
Phospholipase Cβ	PLCβ
Pleckstrin homology	PH
Platelet-derived growth factor	PDGF
Protein kinase A	PKA
Ras-binding domain	RBD
Reverse transcriptase polymerase chain reaction	RT-PCR
Receptor tyrosine kinase	RTK
SH2-domain-containing protein tyrosine phosphatase	SHP-2
Sodium dodecyl sulphate polyacrylamide gel electrophoresis	SDS-PAGE

Src homology 2	SH2
Src homology 3	SH3
Sterol regulatory element binding protein 1c	SREBP-1c
Thin layer chromatography	TLC
Western blot	WB
White adipose tissue	WAT

Acknowledgements

I owe my gratitude to all those people whose help and efforts have made this dissertation possible. First, I would like to sincerely thank my mentor, Dr. Richard Z. Lin, for instilling in me the qualities of being a good scientist. Beyond his guidance and support, his infectious enthusiasm and unlimited zeal have been major driving forces throughout my Ph.D. career. Richard's mentorship has provided me with well-rounded experiences to face challenges in my future career. I am grateful to Dr. Lisa M. Ballou for her guidance. I have learned a lot from her extensive knowledge of the field. Her technical and editorial advices have been valuable as well. I am indebted to all the members of my laboratory, especially Dr. Elzbieta Selinger and Dr. Ya-Ping Jiang, for teaching me some of the experimental techniques.

I would like to thank my committee members for their patience, support and encouragement. Dr. Raafat El-Maghrabi was always there to listen, comfort and give advice. Insightful ideas and constructive criticisms from Dr. Wei-Xing Zong and Dr. Howard Crawford were thought-provoking and they helped me stay focused on my ideas. Dr. Suzanne Scarlata helped and guided me with the fluorescence spectroscopy studies. Dr. Peter Brink provided me with continuous encouragement and support that enriched my graduate school experience.

I will always be grateful to Dr. Stuart McLaughlin for giving me an opportunity to join the doctoral program in the Department of Physiology and Biophysics. I am thankful to the members of Dr. Scarlata's lab, especially Dr. Finly Philip and Dr. Louisa Dowal,

and members of Dr. Zong's lab, especially Dr. Yongjun Fan and Zhixun Dou, for their help and support. I would like to thank Dr. Valentina Schmidt for providing valuable suggestions with the metabolic studies. Special thanks to Melanie Bonnette and Robin Green for taking care of all the graduate students and making sure that we don't have to worry about paperwork. And thanks to Laurie Levine for her technical assistance with mouse handling.

Getting through my dissertation required more than academic support and I am grateful to some close friends for being understanding, encouraging and patient. Being far away from my own family and home country has been quite challenging at times, and they have made me feel at home, away from home.

Most importantly, none of this would have been possible without the love, patience and support of my family. I thank my parents for their faith in me and allowing me to be as ambitious as I wanted to be. It was under their watchful eyes that I gained so much drive and an ability to tackle challenges head on. They gave me my name, my life and everything in between. I am thankful to my brother and sister-in-law for believing in my strengths and being supportive and encouraging. My heart-felt gratitude to my grandparents, whose unwavering faith and confidence in me and my abilities is what has shaped me to be the person I am today. And thanks to everyone else, including my extended family and friends in India, who kept asking me all these years, "Have you completed your thesis yet?" Silencing that question was a prime motivation when intellectual pursuits eluded me.

Publication

1. **Gαq Binds to p110α/p85α Phosphatidylinositol 3-Kinase and Displaces Ras.** Ballou LM, **Chattopadhyay M** et al., Biochem J. 2006 Mar 15; 394; 557-62.

Chapter 1.

Introduction to Phosphatidylinositol-3 Kinase (PI3K)

1-1. GENERAL INTRODUCTION

PI3Ks were first identified in the mid 1980s when researchers found a previously unknown phosphoinositide (PI) kinase associated with the polyoma middle T protein [1]. Subsequent studies by the same group led to the discovery that this PI kinase had a substrate specificity for PI(4,5)P_2 (PIP_2) *in vivo* and was able to phosphorylate it on the 3' position of the inositol ring to generate PI(3,4,5)P_3 (PIP_3) [2] (Fig. 1-1). Although the PIP_3 levels in cells are usually low (0.05 µM in unstimulated neutrophils and 2 µM after treatment with an agonist peptide for 10 seconds) in comparison to PI(4)P (30-40 µM) and PIP_2 (50-35 µM), this lipid second messenger caught the attention of the scientific community because it is capable of transforming mammalian cells [3-4]. It is now well established that deregulated PI3K signaling contributes to the development of diseases such as cancer, autoimmune diseases, neurological diseases, diabetes and metabolic syndrome, to name a few.

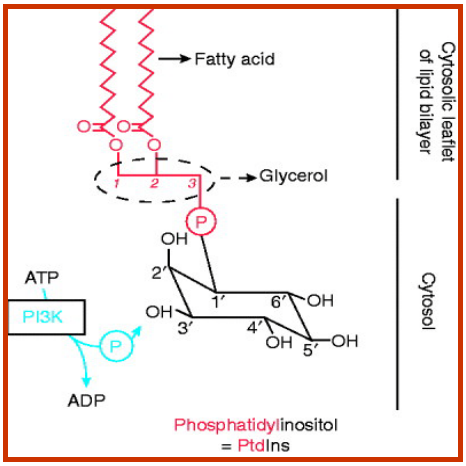

Bart Vanhaesebroeck and D.R. Alessi, Biochem. J., 2000

Fig. 1-1. Generation of PI(3,4,5)P_3 by PI3K. Phosphoinositides (PI) are composed of a membrane-associated phosphatidic acid group that is linked to a cytosolic inositol head group that can be phosphorylated at several positions. PI3Ks can phosphorylate PI(4,5)P_2 (PIP_2) at the D-3 position to form the second messenger PI(3,4,5)P_3 (PIP_3).

1-1-1. Class IA PI3Ks

PI3Ks comprise a group of about 15 proteins. On the basis of their structural and functional homologies, PI3Ks are categorized into classes I, II and III. Class I PI3Ks are further divided into class IA and IB based on their distinct catalytic and regulatory subunits. In mammals three genes have been identified that encode the catalytic subunits of class IA PI3Ks, termed p110α, p110β and p110δ [5-7]. Whereas p110α and p110β are ubiquitously expressed, the p110δ isoform is preferentially expressed in leukocytes. Three additional genes have been described that encode the regulatory subunits. Two genes encode the p85α and p85β isoforms [8-12]. In addition, two smaller proteins (p50α and p55α) come from alternative splicing of the p85α transcript [13-14]. A third gene encodes p55γ [15], which has a structure similar to p55α. In contrast to p85α and p85β that are ubiquitously expressed, the smaller isoforms are distributed in a tissue-specific manner.

Class IA PI3Ks can phosphorylate PI, PI(4)P and PIP_2 *in vitro*, but *in vivo* they preferentially phosphorylate PIP_2. Amino acid substitutions and structural modeling have revealed that the lipid kinase specificity of class IA PI3Ks is dependent on the activation loop sequences (sequences C-terminal to the PI3K ATP-binding site) [16]. In chapter 3 of this thesis, I show that the lipid kinase activities of the different p110/p85 complexes

are not the same and are dependent on the p110 isoform. My results indicate that the kinase activity of the p110α isoform is greater than that of p110β irrespective of the p85 isoform binding partner.

1-1-2. Domain Structure of Class IA PI3Ks

The three catalytic subunits of PI3K are molecules of about 110 kDa that share about 42-58% amino acid sequence homology [5, 17]. At the N terminus they contain a p85-binding domain followed by a Ras-binding domain and a C2 domain that probably mediates binding to phospholipid membranes. Adjacent to the C2 domain is a helical domain that is conserved between members of the PI3K and PI4K superfamilies and members of a more distantly related family of protein kinases that includes mTOR and DNA-PK. At the C terminus the PI3Ks contain a catalytic domain that shares homology to distantly related protein kinases (Fig. 1-2).

The 85 kDa regulatory subunits also share an overall domain structure. The p85α and p85β isoforms contain an N-terminal Src homology 3 (SH3) domain, two or three proline-rich segments, and a break-point cluster homology domain (BHD) that is an area with homology to the GTPase-activating proteins (GAP) of the Rho family of guanine nucleotide-binding proteins (G proteins). The BHD domain does not possess catalytic activity since it lacks five residues that are conserved in the Rho-GAP domains [18]. In the C terminus there are two Src homology 2 (SH2) domains that bind to phosphorylated tyrosines (YXXM motifs) found in activated tyrosine kinase receptors and insulin receptor substrates and a coiled-coil region (iSH2 domain) that binds to the catalytic subunit. This p110-binding region shares 74% homology between the p85α and p85β

subunits. The N-terminal domain in the smaller isoforms (p50α, p55α and p55γ) is replaced by short amino acid sequences (Fig. 1-2).

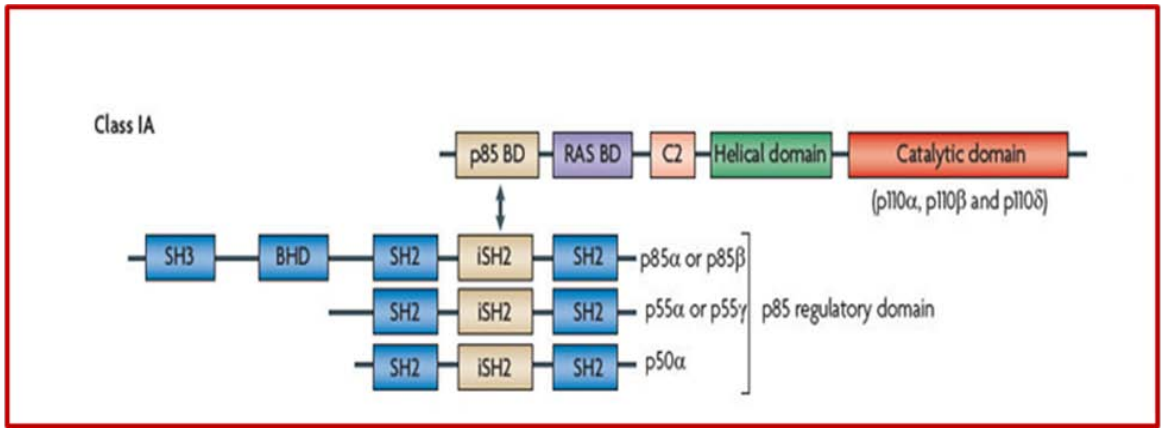

Wu et al., Biochemical Society Transactions, 2007

Fig. 1-2. Domain structures of p110 and p85 PI3K subunits.

The p110 catalytic subunits are constitutively associated with a regulatory p85 subunit. The main function of the regulatory subunit is to recruit the p110 catalytic subunits to tyrosine-phosphorylated proteins at the plasma membrane, where the p110 catalytic subunit phosphorylates its lipid substrate. Evolutionarily, this function of p85 is conserved back to *Drosophila melanogaster*, which expresses a 60 kDa regulatory subunit comprising the SH2 domains and the p110-binding region [19]. Besides regulating the subcellular localization of p110, p85 also stabilizes p110. Monomeric PI3K catalytic subunits are unstable and are rapidly degraded under physiological conditions [20]. To date, there is no evidence for selective associations among any of the catalytic subunits with specific regulatory subunits.

1-1-3. Activation of PI3K

PI3K catalytic activity is tightly regulated in cells by various mechanisms. p110/p85 complexes are present in the cytoplasm of resting cells, ready for activation in response to appropriate cues. One cue comes from ligand-mediated activation of receptor tyrosine kinases (RTKs). Hormones like insulin and growth factors such as insulin-like growth factor 1 (IGF-1) bind to the RTK, causing dimerization and rapid activation of the receptor's cytoplasmic kinase domain. The activated receptor then becomes autophosphorylated on multiple specific intracellular tyrosine residues, and it can phosphorylate tyrosine residues on substrates such as the insulin receptor substrate (IRS) proteins. Interaction of the SH2 domain of p85 with the phosphotyrosine residues on the RTK (or with the IRS proteins) recruits the p110/p85 complex to the receptor and activates the complex (Fig. 1-3).

Besides RTKs, PI3K can also be activated by Ras proteins. Ras proteins belong to the superfamily of monomeric GTPases, which are involved in receptor-mediated signal transduction pathways. Other members of the family are Rho GTPase, a remodeller of the actin cytoskeleton, and Rab GTPase, a regulator of intracellular trafficking. In mammals, there are four types of Ras proteins: H-Ras, N-Ras and K-Ras, with K-Ras existing in two variants, K-Ras4A and K-Ras4B, due to alternative splicing. Ras proteins are located on the inner surface of the plasma membrane and attached to the membrane by a farnesyl residue. Ras proteins transmit extracellular signals that promote the growth, proliferation, differentiation and survival of cells. The signaling cascade starts from the plasma membrane where the growth factor (e.g. epidermal growth factor (EGF), FGF) binds to its enzyme-linked receptor causing receptor dimerization. This leads to phosphorylation

of the intracellular parts of the receptors, which activates guanine exchange factors (GEF), such as sos. GEFs are attached to the receptor by the adaptor proteins shc and grb-2. GEFs promote the exchange of GDP attached to inactive Ras to GTP, which leads to activated Ras. Ras-GTP is constantly inactivated by Ras-GAP proteins (e.g., NF1 protein, p120GAP), which promote the intrinsic GTPase of Ras. This leads to the hydrolyzation of active Ras-GTP into inactive Ras-GDP. The major downstream target of Ras-GTP is mitogen-activated protein kinase (MAPK). Activation of MAPK occurs through specific phosphorylation of both a threonine and a tyrosine separated by a single amino acid. The first component of MAPK is called Raf, which is activated on the plasma membrane by Ras-GTP. Raf phosphorylates mitogen-activated kinase 1/2 (MEK1/2 kinase), which activates the extracellular regulated kinase 1/2 (ERK1/2 kinase or p44/42 MAPK) by phosphorylation. ERK1/2 kinase phosphorylates a variety of downstream targets, which results in changes in gene expression and the catalytic activities of enzymes. There are two other signaling pathways related to MAPK. These are called p38 MAPK and c-Jun N-terminal kinase/stress-activated protein kinase (JNK/SAPK), and they are mainly involved in transmitting inflammatory signals. PI3K is another well known downstream effector of Ras. Purified H-Ras protein was reported to bind directly *in vitro* to purified PI3K (p110α/p85α) in a GTP-dependent manner [21]. The affinity of the interaction of H-Ras·GTP with this complex was reported to be approximately 150 nM [22]. In chapter 3 of this thesis, I show that the class IA PI3K complexes p110β/p85α, p110α/p85β, and p110β/p85β are also able to bind to activated Ras proteins. Using mutation analysis, the site of interaction on the p110 catalytic subunit was found to be the Ras-binding domain (RBD) [22]. The homology over the RBD region is 25% between p110α and β, 18%

between p110α and γ and 20% between p110β and p110γ. It has been suggested that the interaction of Ras·GTP with the PI3K catalytic subunit plus binding of the PI3K regulatory subunit to phosphotyrosine residues synergize to fully activate PI3K.

Contrary to the extensive research on activation of PI3K, there is very limited understanding of how the activated PI3K complex is downregulated. One hypothesis is that tyrosine phosphorylation of p85, which occurs after the p110/p85 complex has been recruited to the receptor, serves as a negative regulatory signal that leads to a reduction in the p110 catalytic activity [23].

1-1-4. PI3K signaling pathways

Generation of PIP_3 by PI3Ks activates a highly complex web of downstream signaling networks to regulate different cellular responses. PIP_3 can bind and recruit pleckstrin homology (PH) domain-containing proteins to the inner leaflet of the cell membrane. The best known downstream target of PIP_3 is the protein Ser/Thr kinase Akt. Binding of PIP_3 to the PH domain of Akt is required for the phosphorylation of both Thr308 and Ser473 on Akt, resulting in its complete activation [24]. Akt is believed to be involved in the regulation of cell growth, proliferation, cell survival, metabolism, transcription and protein synthesis (Fig. 1-3). The level of PIP_3 is decreased by phosphatases such as PTEN (phosphatase and tensin homologue deleted on chromosome ten), a tumor suppressor which induces cell cycle arrest and promotes apoptosis. PTEN down-regulates PI3K signaling by dephosphorylating PIP_3 at the D-3 position. (Fig. 1-3).

The specificity of the cellular responses following activation of the PI3K signaling pathway depends on the cellular stimuli, the PI3K isoform and/or the effector

proteins that transmit the signal. Most of the physiological effects of insulin are thought to be mediated by class IA PI3K/Akt signaling pathways. Insulin regulates carbohydrate, lipid and protein metabolism to maintain normal glucose and lipid homeostasis. Insulin increases glucose uptake in muscle and fat, and inhibits glucose production and glycogen breakdown in the liver, thus serving as the primary regulator of blood glucose concentration. Glycogen synthase kinase-3 (GSK3) is one of the direct substrates of Akt. In response to insulin activation of PI3K/Akt, phosphorylation of GSK3 decreases its activity towards glycogen synthase, which leads to increased glycogen synthesis. Insulin-dependent changes in glucose production are controlled at the gene expression level. Transcription of genes encoding the enzymes phosphoenolpyruvate carboxykinase (PEPCK) and glucose 6-phosphatase (G6PC) that govern the rate-limiting steps in glucose production are regulated by PI3K. To maintain normal lipid homeostasis, insulin stimulates fatty acid and triglyceride synthesis in the liver and inhibits lipolysis in adipose tissue. Changes in expression of lipogenic genes such as sterol regulatory element binding protein 1c (SREBP-1c) and fatty acid synthase (FAS) are also mediated by the PI3K signaling pathway. Besides Akt, Ser/Thr kinases downstream of PI3K include the atypical PKCs (including PKC λ and ζ). Unlike the other classes of PKC, atypical PKCs (aPKC) are not activated by diacylglycerol and Ca^{+2}. In response to insulin activation of PI3K, increased levels of PIP_3 bind to and activate aPKCs. aPKCs mediate insulin-dependent increases in lipid synthesis. Insulin also stimulates cell growth and differentiation and protein synthesis *via* PI3K through activation of mTOR (mammalian target of rapamycin). mTOR regulates protein synthesis by phosphorylating the 70 kDa

ribosomal protein S6 kinase (p70S6K), which in turn phosphorylates ribosomal protein S6.

Since the PI3K pathway is critical for regulating multiple cell processes, it is not surprising that deregulation of this pathway can contribute to the development of diseases. In fact, attenuated PI3K signaling downstream of the insulin receptor is a major contributor toward metabolic syndrome and type 2 diabetes, whereas amplification of PI3K signaling is one of the most common causes of human cancers.

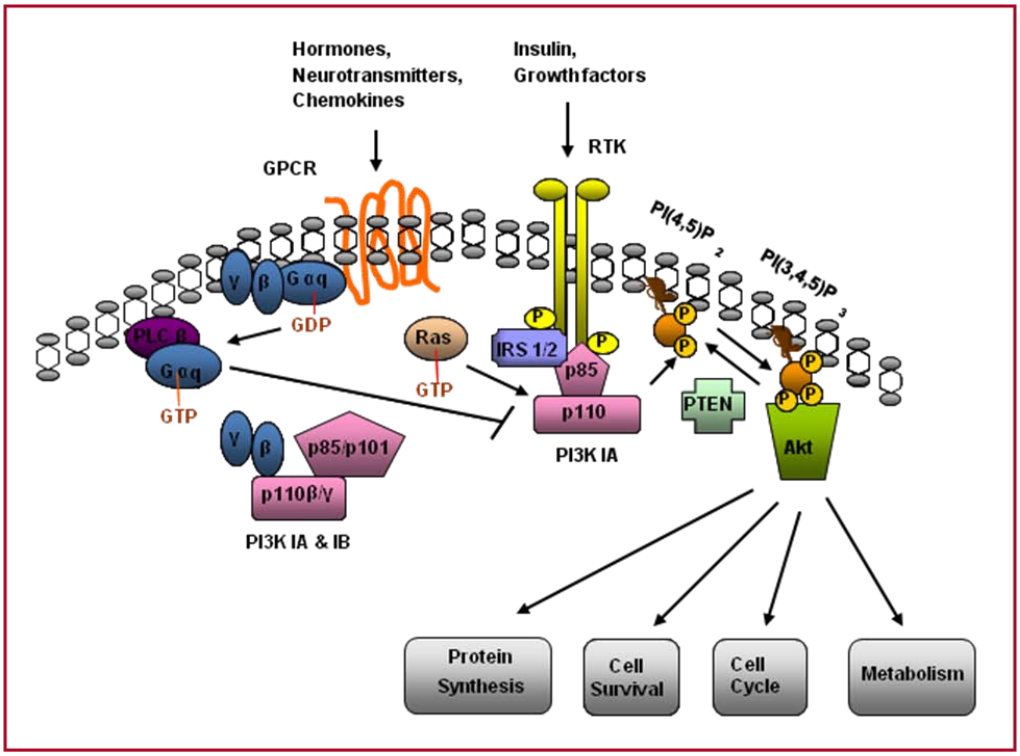

Fig. 1-3. The PI3K signaling pathway. Hormone binding to the receptor tyrosine kinase (RTK) or activation of Ras activates the p110/p85 complex of class IA PI3K. PI3K phosphorylates PIP_2 to generate PIP_3 on the cell membrane that activates the downstream effector Akt. Akt regulates protein synthesis, cell survival, cell cycle and metabolism. Hormone binding to the G protein-

coupled receptor (GPCR) activates $G\alpha_q$, resulting in exchange of GTP for GDP as well as dissociation of Gβγ. Activated $G\alpha_q$ activates phospholipase C **(**PLC) β and inhibits class IA PI3K. Gβγ binds to p110β (class IA PI3K) and p110γ (class IB PI3K) and activates them. IRS 1/2, insulin receptor substrate 1/2; PTEN, phosphatase and tensin homolog deleted on chromosome ten; P, phosphorylation.

1-1-5. Regulation of PI3K by G proteins

G proteins are signal transducers that connect cell surface receptors to intracellular signaling pathways. Heterotrimeric G proteins consist of 3 subunits α, β and γ. Currently there are twenty known Gα, six Gβ and eleven Gγ subunits. On the basis of sequence similarity, the Gα subunits have been divided into four families—$G\alpha_q$, $G\alpha_s$, $G\alpha_{i/o}$ and $G\alpha_{12/13}$. $G\alpha_q$ is ubiquitously expressed in all tissues. The $G\alpha_q$ family members have been implicated in the regulation of cell growth and proliferation, neuronal signaling, platelet aggregation, glucose secretion, embryonic development and smooth muscle contraction. Many extracellular agents such as hormones, neurotransmitters and chemokines, through the activation of seven transmembrane cell surface receptors, activate $G\alpha_q$. Activation promotes the exchange of GDP for GTP on the Gα subunit and triggers the dissociation of the Gβγ heterodimer [25], [26] (Fig. 1-3). The intrinsic GTPase activity of Gα hydrolyzes GTP to GDP to inactivate itself. The best known downstream effector of $G\alpha_q$ is phospholipase C (PLC) β, which hydrolyzes PIP_2 to release inositol (1,4,5) trisphosphate and diacylglycerol (DAG). These second messengers further activate distinct downstream signaling pathways, including calcium release and PKC, respectively. $G\alpha_s$ activates the cAMP-dependent pathway by stimulating the production

of cAMP from ATP. This is accomplished by direct stimulation of the membrane-associated enzyme adenylyl cyclase. cAMP acts as a second messenger that goes on to interact with and activate protein kinase A (PKA). PKA can then phosphorylate a myriad of downstream targets. On the other hand, $G\alpha_i$ inhibits the production of cAMP from ATP. Some of the effectors of $G\alpha_{12/13}$ are Bruton's tyrosine kinase, protein phosphatase 2A and E-cadherin [27-29].

Following receptor activation, the $G\beta\gamma$ heterodimers can also function as signaling molecules independently of the $G\alpha$ subunit (Fig. 1-3). Besides activation by RTKs, multiple studies have shown that PI3K p110β can also be activated by G protein-coupled receptors (GPCRs) through $G\beta\gamma$ [30-33]. In fact, synergistic activation of p110β following stimulation of the two major receptor types was observed in differentiated THP-1 cells, CHO cells and rat adipocytes [34]. On the other hand, there is no evidence that PI3K p110β can affect heterotrimeric G protein signaling pathways. In chapter 2 of my thesis, I will show that p110β is involved in regulating the expression of adenylyl cyclase, the canonical effector of $G\alpha_s$.

The data regarding the regulation of PI3K by $G\alpha_q$ have been controversial. Depending on the cellular context, some $G\alpha_q$-coupled receptors either activate [35], [36] or inhibit the PI3K signaling pathway [37]. Our laboratory found that activation of $G\alpha_q$ through the α_{1A} adrenergic receptor inhibits PI3K signaling [37]. Several growth factors including insulin and IGF-1 generate survival signals and prevent cell death *via* the activation of Akt. Expression of activated $G\alpha_q$ in COS-7 and CHO cells induces apoptosis [38]. Thus, inhibition of Akt may be the mechanism by which activated $G\alpha_q$ induces apoptosis [38], [39]. The inhibitory effect of $G\alpha_q$ on Akt activation raised the

possibility that activated $G\alpha_q$ might have a direct inhibitory effect on its upstream regulator, PI3K. In chapter 3 of this thesis, I tested this hypothesis using purified $G\alpha_q$ and PI3K proteins.

Chapter 2.

Ablation of PI3K p110α prevents high-fat diet-induced liver steatosis and deletion of p110β induces hyperglycemia by increasing cellular cAMP Levels

2-1. INTRODUCTION

The liver is a hormone-responsive organ that plays a role in maintaining whole body lipid and glucose homeostasis. After feeding, insulin levels rise and excess glucose is stored as glycogen in the liver. During times of fasting, glucagon and catecholamine levels rise to increase the cAMP level in hepatocytes. This leads to the breakdown of glycogen to produce glucose (glycogenolysis) and to the *de novo* synthesis of glucose (gluconeogenesis). The liver also maintains lipid homeostasis by *de novo* lipogenesis to produce fatty acids as an energy source for other organs and by taking up and storing excess lipids as triglycerides in the liver. Hence it is not surprising that defects in hepatic metabolic regulation can contribute to the development of metabolic syndrome and type 2 diabetes mellitus.

Both lipid and glucose metabolism in the liver are regulated by class IA PI3Ks [40-41]. PI3Ks produce PIP_3, which is required for the activation of downstream effectors such as Akt and atypical protein kinase C (aPKC) λ and ζ [24, 42]. Results from studies using genetically modified mice suggest that Akt primarily regulates glucose metabolism in the liver [43-44] whereas hepatic lipid metabolism is mainly regulated by aPKCs [45]. Current evidence suggests that the aPKC pathway positively regulates the transcription factor sterol regulatory element binding protein 1c (SREBP-1c) which is a major regulator of lipid synthesis [46]. On the other hand, the Akt signaling pathway appears to negatively regulate the major gluconeogenic genes phosphoenolpyruvate carboxykinase (PEPCK) and glucose 6-phosphatase (G6PC) [44].

Liver steatosis affects 34% of the US population between the ages of 30 and 65, making it the most common liver disorder. Although some drugs and genetic abnormalities can cause fatty liver, the majority of cases are associated with obesity and type 2 diabetes. Liver steatosis may progress to steatohepatitis, which leads to fibrosis and cirrhosis. Liver steatosis is characterized by the accumulation of excess hepatic triglycerides resulting from an imbalance between uptake, export, synthesis and oxidation of fatty acids. It is well established that high-fat diets (HFD) can induce hepatic steatosis in humans and rodents, but the mechanism of lipid accumulation is unclear. HFD causes an increase in expression of gluconeogenic genes as well as a paradoxical increase in the expression of lipogenic genes, SREBP-1c and PPARγ in mouse liver [47-48]. It would seem counterintuitive to have increased lipogenesis in the face of excess dietary fats, and some studies have shown that HFD-induced liver steatosis can be blocked without inhibiting *de novo* lipogenesis [49]. Another possible explanation for high triglyceride accumulation in the liver could be increased uptake of fatty acids from the blood. Fatty acid uptake in the liver is mediated by several transport proteins, including the fatty acid transporter protein, fatty acid translocase and the highly expressed liver fatty acid binding protein (L-FABP). Genetic deletion of L-FABP in mice caused a decrease in fatty acid uptake in the liver that protected them from HFD-induced liver steatosis [50]. Currently, it is unknown if PI3Ks regulate hepatic fatty acid uptake.

In this chapter, I studied the roles of PI3K p110α and p110β in lipid and glucose metabolism using liver-specific gene targeting in mice. I show that ablation of p110α, but not p110β, attenuated liver steatosis induced by a HFD. Surprisingly, the p110β-null mice

exhibited alterations in glucose metabolism that may be due to increased intracellular cAMP levels and not to changes in Akt signaling.

2-2. MATERIALS AND METHODS

Materials

Antibodies were purchased from the following sources: for p110α from BD Biosciences; for p110β, Akt, IRS-1 and S6 from Santa Cruz Biotechnology; for pan-p85 and GSK3β (glycogen synthase kinase 3β) from Millipore; for phospho-Akt, phospho-GSK3β, phospho-S6, and fatty acid synthase (FAS) from Cell Signaling; and for L-FABP (fatty acid binding protein) from Abcam.

Animals

To generate *p110α*Flox/Flox mice, a 11.6 kb region used to construct the targeting vector was first subcloned from a BAC clone. The region was designed so that the short homology arm extended 1.62 kb 3' to exon 1. The long homology arm ended 5' to exon 1 and was 8.2 kb long. The *loxP*- and *FRT*-flanked Neo cassette was inserted on the 3' side of exon 1 and a third *loxP* site was inserted at the 5' side of exon 1. The target region was 1.85 kb and included exon 1. To generate *p110β*Flox/Flox mice, the 14.6 kb region used to construct the targeting vector was first subcloned from a BAC clone. The region was designed so that the short homology arm extended 2 kb 3' to exon 4. The long homology arm ended 5' of exon 3 and was 7.8 kb long. The *loxP*- and *FRT*-flanked Neo cassette was inserted on the 3' side of exon 4 and a third *loxP* site was inserted at the 5' side of exon 3. The target region was 4.8 kb and included exons 3 and 4. The targeting constructs were electroporated into embryonic stem cells. G418 selection was applied for 10 days and clones were screened by PCR for targeted integration of the Neo selection marker

and the presence of the third *loxP* site. Targeted clones were microinjected into C57BL/6 blastocysts and resulting chimeras were identified by coat color. Chimeras with a high percentage of agouti color were mated with C57BL/6 WT mice. Germline transmission was confirmed in agouti pups by PCR to detect the targeted integration of the Neo cassette and the presence of the third *loxP* site. These mice were then bred with *rosa26-FLP* mice (Jackson Laboratories) to remove the Neo cassette flanked by *FRT* sites. Genotyping to detect homozygosity of the floxed genes in *p110α*Flox/Flox and *p110β*Flox/Flox mice was done by PCR analysis of tail DNA using primers that span one of the *loxP* sequences (if present). Reactions from the floxed alleles yielded a 450 bp band, whereas the product from the WT alleles was a 240 bp band. The generation of $p110\alpha^{loxp/loxp}$ and $p110\beta^{loxp/loxp}$ mice is also described previously [51]. We bred these mice to hepatocyte-specific albumin-Cre (*Alb-Cre*) transgenic mice to produce liver-specific p110α and p110β knockout mice. The one copy of the *Alb-Cre* gene in both mouse lines was detected by primers that span part of the *Cre* sequence. To avoid potential variations due to gender, only male mice were used. $p110\alpha^{loxp/loxp}$; Alb-Cre^{+} mice (referred to as $p110\alpha^{-/-}$) were compared to $p110\alpha^{loxp/loxp}$ (referred to as $p110\alpha^{+/+}$) littermates and $p110\beta^{loxp/loxp}$; Alb-Cre^{+} mice (referred to as $p110\beta^{-/-}$) were compared to $p110\beta^{loxp/loxp}$ (referred to as $p110\beta^{+/+}$) littermates in this study.

These mice were analyzed between 8-16 weeks of age. All animals were housed on a 12-hour light/12-hour dark cycle. For the HFD experiments, 8 week old mice were singly housed and fed either a HFD (45 kcal% fat) from Research Diets, Inc., or standard rodent chow for 8 weeks. The food and water were consumed *ad libitum* throughout the experiment. Body weight was measured once a week. Food intake was monitored weekly.

Prior to the start of the study and at the end of the study, DEXA (Dual Energy X-Ray Absorptiometry) scanning was performed using the PIXImus2 DEXA scanner (Faxitron X-ray Corporation, Wheeling, IL) to determine body fat content. All mice were weighed and anesthetized before scanning.

All animal-related experimental protocols were approved by the Stony Brook University Institutional Animal Care and Use Committee.

In vivo Insulin Signaling

After an overnight fast, mice were injected intraperitoneally with 2 U/kg body weight of human insulin (Novolin; Novo Nordisk) or an equal volume of saline. At different time points after insulin or saline injection, mice were sacrificed and livers were removed and frozen in liquid nitrogen. Liver extracts were subjected to SDS-PAGE and immunoblotted with different antibodies to analyze insulin signaling pathway molecules as previously described [52].

Phosphopeptide Pull-Down of PI3K and Western Blotting

For PI3K pull-downs, liver lysates were prepared in buffer containing 50 mM HEPES, pH 7.5, 10 mM 2-glycerophosphate, 0.1% Triton X-100, 20 mM NaF, 2 mM EDTA, 1 mM benzamidine, 0.1 mM dithiothreitol, 100 mM NaCl, 0.2 mM sodium orthovanadate, and a cocktail of protease inhibitors. Equal quantities of lysate protein (Bio-Rad Protein Assay) were incubated for 2 h at 4°C with phosphopeptide coupled to agarose (CDMSKDESVDYpVPMLDMK; Alpha Diagnostic International). After 4 washes, the beads were boiled in SDS sample buffer and the released proteins were subjected to

Western blotting. Purified p110α/p85α, p110β/p85α and p110δ/p85α were run as controls and the blot was probed with antibodies to p110α (BD Biosciences), p110β (Santa Cruz Biotechnology), p110δ (Santa Cruz) and pan-p85 (Millipore). Signals were visualized using horseradish peroxidase-linked secondary antibodies (Amersham Biosciences) and chemiluminescence reagents (PerkinElmer Life Sciences) [51].

IRS-1 Pull-Down of PI3K

Overnight fasted mice were anesthetized and injected through the inferior vena cava with insulin (2 U/kg). Liver extracts were incubated overnight at 4^{o}C with anti-IRS-1 antibody and the immunocomplexes were pulled down by protein A agarose and washed with the lysis buffer followed by a PI3K activity assay.

Kinase Assays

Overnight fasted mice were injected intraperitoneally with 2 U/kg of insulin or saline. Liver extracts were subjected to *in vitro* Akt, aPKC and PI3K activity assays in the absence or presence of 500 nM PI-103, 50 nM TGX-221, 5 μM IC87114 or vehicle as previously described [52-53].

For PKCζ activity equal amounts of lysate protein were incubated with anti-PKCζ antibody (Transduction Laboratories) for 3 h on ice and then with protein G-agarose for 1 h. Following extensive washing, the reaction was initiated with 25 μl of assay buffer containing 50 mM Tris, pH 7.5, 5 mM MgCl2, 1 mM NaHCO3, 1 mM phenylmethylsulfonyl fluoride, 40 μg/ml phosphatidylserine, 40 μM ATP, 2.5 μCi of

[γ-32P]ATP, and 40 μM [Ser159]PKCζ-(149–164) substrate peptide (Quality Controlled Biochemicals). The reactions were incubated for 10 min at 30 °C. An aliquot was spotted onto P-81 phosphocellulose paper, and following extensive washing with 75 mM phosphoric acid, radioactivity on the papers was quantified by scintillation counting.

For Akt activity, liver extracts were lysed with lysis buffer (50 mM Tris, pH 7.5, 120 mMNaCl, 1% Nonidet P-40, 1 mM EDTA, 50 mM NaF, 40 mM 2-glycerophosphate, 0.1 mM sodium orthovanadate, 1 mM benzamidine, 0.5 mMphenylmethylsulfonyl fluoride, and 10 μg/ml aprotinin and leupeptin) and insoluble material was removed by centrifugation. Equal amounts of lysate protein were incubated with antibody against Akt (Upstate) overnight at 4 °C and then with 20 μl of protein A-agarose (Santa Cruz Biotechnology, Santa Cruz, CA) for 1 h. The beads were washed 2 times with lysis buffer and once with Akt assay buffer (50 mM Tris, pH 7.5, 10 mMMgCl_2, 1 mM dithiothreitol, 1 mMbenzamidine and 0.5 mM phenylmethylsulfonyl fluoride). The washed immunocomplexes were resuspended in 25 μl of Akt assay buffer containing 40 μM ATP, 2.5 μCi of [γ-^{32}P]ATP, 1 μM protein kinase A inhibitor peptide (Sigma), and 100 μM Akt peptide substrate (Santa Cruz Biotechnology). The reaction mixture was incubated for 30 min at 30 °C, and then an aliquot was spotted onto P81 phosphocellulose paper. Following extensive washing in 75 mM phosphoric acid, radioactivity on the papers was quantified by scintillation counting. Protein concentration of cell lysates was determined using a Bradford assay (Bio-Rad).

To measure PI 3-kinase activity, liver lysate was incubated with 4 μg of PY20 phosphotyrosine antibody (Transduction Laboratories, Lexington, KY) overnight at 4°C and then with 20 μl protein A-agarose for 1 h. The beads were washed twice with lysis

buffer and twice with PI 3-kinase assay buffer (20 mM Hepes, pH 7.5, 100 mM NaCl, and 50 μM EDTA). The washed beads were resuspended in 50 μl of kinase reaction buffer (20 mM Tris-HCl, pH 7.5, 100 mM NaCl, and 0.5 mM EGTA) and incubated at room temperature for 10 min after addition of phosphatidylinositol dissolved in chloroform. The micelles of PI were produced by sonication in assay buffer. Reactions were initiated with addition of 5 μl of ATP solution (0.4M ATP, 0.1 M $MgCl_2$, and 1 μCi/ml [γ-^{32}P]ATP) and continued at room temperature for 30 min. During this period, the formation of phosphatidylinositol phosphate was linear (data not shown). The reaction was stopped after the addition of 100 μl of chloroform /methanol/11.6 N HCl (100:200:2). Following centrifugation, the lower organic phase was taken and separated by thin layer chromatography on Silica Gel plates developed in chloroform, methanol, 25% ammonium hydroxide, and water (43:38:5:7). The plates were visualized by autoradiography and quantified by a PhosphorImager (Molecular Dynamics).

Estimation of Tissue Triglyceride Content

Mice fasted for 6 hours were sacrificed and tissues were frozen in liquid nitrogen. Frozen tissues (20-100 mg) were homogenized in phosphate buffered saline (PBS) and extracted with chloroform and methanol (3:1). The extracts were dried overnight and resuspended in 100% isopropanol. An appropriate volume of the suspension was assayed using a triglyceride assay kit from Sigma-Aldrich.

Hepatocyte Isolation

Primary hepatocytes were isolated from mice of the indicated genotype by collagenase perfusion of the liver as previously described by Seglan [54]. In brief, under anesthesia with ketamine/xylazine (intraperitoneal), the liver was perfused first with Krebs Ringer buffer (122 mM NaCl, 5.6 mM KCl, 5.5 mM D-glucose, 2.5 mM $NaHCO_3$ and 20 mM Hepes, pH 7.4) with 0.1 mM EGTA, followed by perfusion with Krebs Ringer buffer with 1.37 mM $CaCl_2$ and 28 mg/50 ml of collagenase (Worthington, type I). Both buffers were run at 5 ml/min for 10 min each. Hepatocytes were harvested and viability was examined by trypan blue exclusion. Isolated hepatocytes were plated on collagen-coated plates in DMEM/F12-Ham's medium (Sigma) supplemented with 10% fetal bovine serum, 1% antibiotic/antimycotic reagent (Sigma), 1 g/L of fatty acid free bovine serum albumin (BSA) (Sigma), and 1×Insulin-Selenium-Transferrin (Gibco). Cells were allowed to recover overnight before using them for experiments. All mice used in the isolation of hepatocytes were fed a normal chow diet.

Long Chain Fatty Acid Uptake

Isolated hepatocytes were incubated with increasing concentrations of [^{3}H]palmitate bound to defatted BSA in a constant 3:1 molar ratio in PBS at 37^{o}C. After 1 min, the uptake was stopped by adding 200 μM phloretin/0.1% BSA at 4^{o}C to the cells. The cells were washed 3 times with ice-cold PBS and lysed in lysis solution (0.1 M NaOH, 0.03% SDS) and protein content was measured using the BCA assay from Thermo Scientific. Cellular uptake of [^{3}H]oleate was determined directly by cell-associated radioactivity and normalized to the total protein concentration.

Metabolic Studies

For glucose tolerance tests, mice fasted overnight were injected intraperitoneally with 2 g/kg of dextrose and blood glucose was measured at 0, 30, 60 and 120 min. The pyruvate challenge test was performed in animals fasted overnight by injecting 2 g/kg of pyruvate (Sigma) intraperitoneally, followed by blood collection at 0, 30, 60 and 120 min. Blood glucose measurements were determined using a One Touch Ultra Mini glucose monitor (Lifespan Inc., Millipitas, California). Serum insulin levels were measured by ELISA using mouse insulin as a standard (Crystal Chem Inc., Chicago, Illinois). The serum levels of liver enzymes, bilirubin, cholesterol, triglyceride, albumin and total protein were measured by Anilytics (Gaithersburg, Maryland).

Analysis of Tissue Glycogen Levels

Mice fasted for 6 hours were sacrificed and tissues were frozen in liquid nitrogen. Frozen tissues (20-100 mg) were digested in 30% KOH for 20 min at 100^{o}C. Macromolecules were precipitated by the addition of two volumes of 100% ethanol followed by overnight incubation at -20^{o}C. The next day the samples were centrifuged at 3000 rpm for 15 min at 4^{o}C and the supernatant was removed. Macromolecules were resuspended in water and precipitated again by addition of two volumes of 100% ethanol and incubating overnight at -20^{o}C. Macromolecules were washed in 70% ethanol and glycogen was hydrolyzed by digestion in 84% H_2SO_4. Glucose in the samples was determined colorimetrically as compared to the standards after the addition of anthrone to the samples and standards. Standards contained known concentrations of glucose.

Measurement of Hepatocyte Glucose Production

Hepatocytes isolated from *ad lib* fed mice were treated with or without 10 μM dibutyryl cAMP and 50 nM dexamethasone either in the absence or presence of 2 mM sodium pyruvate and 0.2 mM lactate and incubated at 37^{o}C in glucose-free serum-free medium for 5 h. The culture medium was subsequently collected and glucose was measured using a glucose assay kit from BioVision Inc. and normalized to total protein concentration. Cells were lysed with lysis solution (0.1 M NaOH, 0.03% SDS and protease inhibitors) and protein content was measured using the BCA assay. Glucose production in the presence of the gluconeogenic substrates (pyruvate and lactate) was considered as the total glucose production and glucose production in the absence of pyruvate and lactate was considered as glycogenolysis. Glucose production *via* gluconeogenesis = total glucose production – glucose production by glycogenolysis.

Cyclic AMP Assay

Hepatocytes were preincubated overnight at 37^{o}C with 250 nM 3-isobutyl-1-methylxanthine and then treated with or without 10 μM forskolin for 15 min. cAMP accumulation in hepatocytes was measured by competition binding as previously described [55]. Briefly, cells were lysed with 100% ice cold ethanol. Cells were scraped and aliquots of samples were dried under vacuum and reconstituted with 20mMphosphate buffer (pH 6.0). [^{3}H]cAMP (0.5 pmol) was added to each sample as an internal standard to compete with unlabeled cAMP for the binding to bovine adrenal binding protein. The unbound cAMP was then removed by the addition of activated charcoal. The

radioactivity in the protein-bound cAMP was measured by liquid scintillation counting. A standard curve was generated by plotting the radioactivity vs. the $\log_{10}$ concentration of cAMP. cAMP levels in samples were extrapolated from the standard curve.

Quantitative Reverse Transcriptase (RT)-PCR Analysis

Quantitative RT-PCR analysis was performed as described previously [56]. Total RNA was extracted from livers using Tri Reagent (Sigma) following the protocol provided by the manufacturer. cDNA was generated using the iScript cDNA Synthesis kit (Bio-Rad) following the protocol provided by the manufacturer. TaqMan® Universal PCR Master Mix and TaqMan® gene expression assays for FAS (Mm00662312_g1), Srebf1 (Mm00550338_m1), Pparγ (Mm01184323_m1), Acaca (Mm01314285_m1), fabp1 (Mm00444340_m1), Adcy5 (Mm00674122_m1), Adcy6 (Mm00475772_m1), Pck1 (Mm01247057_g1), G6pc (Mm00839363_m1), and 18 S RNA (HS99999901_s1) (housekeeping gene) were purchased from Applied Biosystems (Foster City, CA). Real-time PCR was performed on duplicate samples using a DNA Engine Opticon 2 System (MJ Research, Alameda, CA). The abundance of mRNA of the gene of interest relative to 18 S RNA was determined using the equation $r = 2^{(C_{T\text{18 S RNA}} - C_{T\text{gene of interest}})}$, where C_T is the number of cycles needed to achieve a preset threshold value of fluorescence. The results are expressed as fold change in r values as compared with control samples.

Histology

Tissues were formalin fixed and embedded in paraffin using standard procedures. Sections (5 μm) were cut and stained with either H&E for standard microscopy or

Periodic Acid-Schiff's reagent to detect liver glycogen. Frozen liver sections (8 μm) were stained with Oil Red O (Sigma) and counterstained with hematoxylin to visualize lipids in the liver.

Statistical Analysis

Student's t-test was used for statistical analysis between groups. All data were subjected to statistical analysis by Excel Analysis Tool (Microsoft). All data are represented either as means ± SEM or % of control. A p value < 0.05 was considered to be significant.

2-3. RESULTS

2-3-1. Ablation of hepatic p110α but not p110β blocks high-fat diet (HFD)-induced liver steatosis

Hepatocyte-specific p110α- and p110β-deficient mice were generated as described in Methods. Extracts of control and knockout livers were analyzed by western blotting to confirm that p110α or p110β was appropriately ablated (Fig. 2-1a). Western blotting also confirmed that the gene deletion was specifically targeted to the liver (Fig. 2-1b). Both knockout mouse strains appeared normal and were fertile. At 9 weeks of age, there were no significant differences between control and knockout animals in body weight, liver protein content, or serum biochemical parameters that assess liver function (Table 2-1). However, the liver weight to body weight ratio and the liver triglyceride content of $p110\alpha^{-/-}$ mice were both significantly decreased as compared to $p110\alpha^{+/+}$ mice (Table 2-1). These values were not significantly different between $p110\beta^{+/+}$ and $p110\beta^{-/-}$ mice (Table 2-1). Gross examination of livers from 9 week-old mice revealed that the general lobular architecture of the organ was preserved in both knockout mouse strains. Histological analysis revealed that there were no obvious abnormalities such as necrosis or fibrosis seen on the liver sections. However closer examination of the liver sections stained with hematoxylin and eosin (H&E) revealed that only the $p110\alpha^{-/-}$ mice lacked small vacuoles with glassy like appearance which could be lipid droplets (Fig. 2-1c).

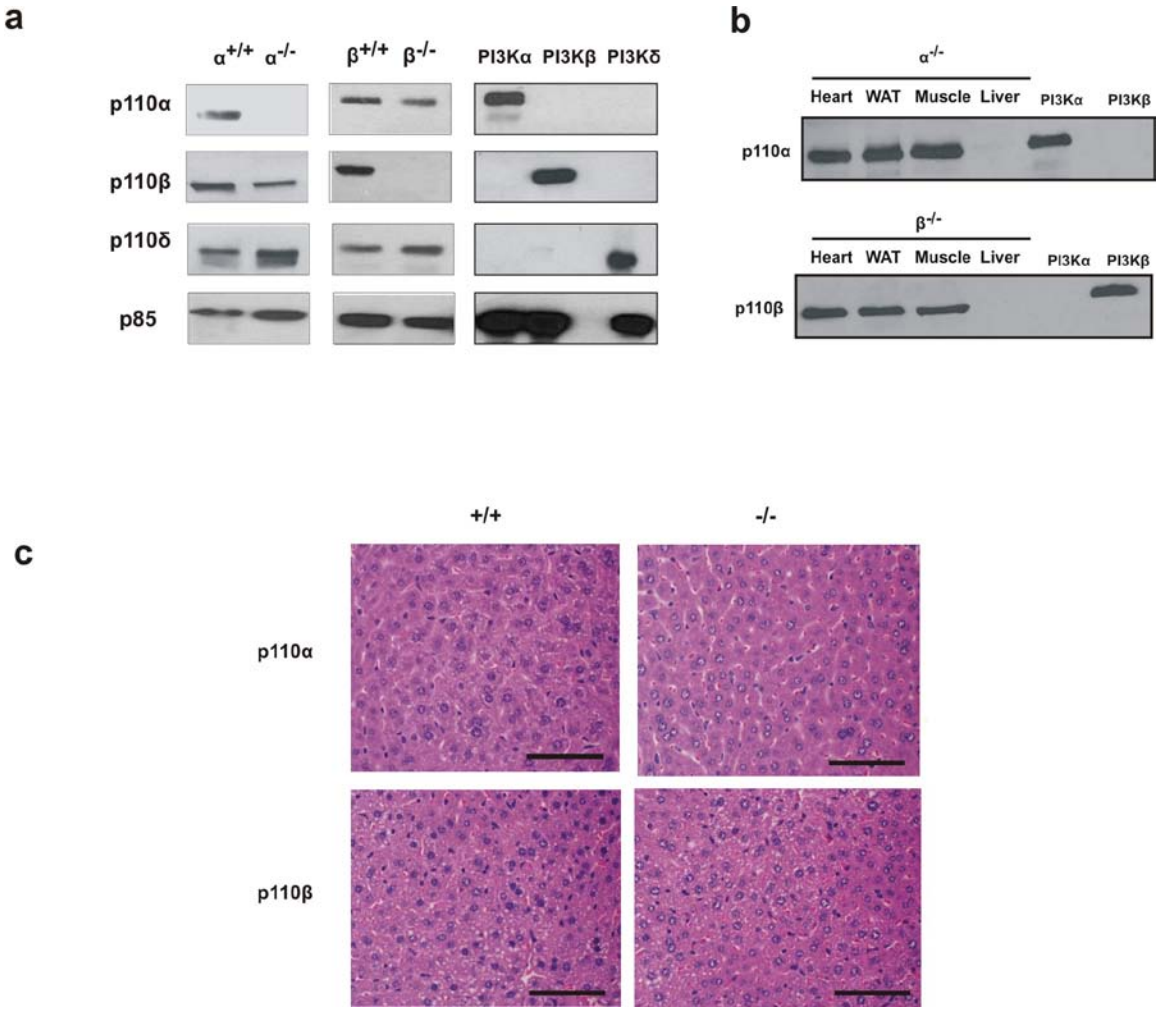

Fig. 2-1. Targeting p110α and p110β PI3K in the liver. (a) Class IA PI3Ks in liver lysates from mice of the indicated genotypes were pulled down with a phosphotyrosine peptide and the bound proteins were examined on western blots probed with the indicated antibodies. Recombinant PI3Kα (p110α/p85α), PI3Kβ (p110β/p85α), and PI3Kδ (p110δ/p85α) were loaded as controls. (b) Class IA PI3Ks in lysates from heart, white adipose tissue (WAT), muscle and liver of $p110\alpha^{-/-}$ and $p110\beta^{-/-}$ mice were pulled down with a phosphotyrosine peptide and the bound proteins were examined on western blots probed with the indicated antibodies. Recombinant PI3Kα (p110α/p85α) and PI3Kβ (p110β/p85α) were loaded as controls. (c) Representative H&E staining of liver sections from mice of the indicated genotypes. Scale bars = 200 μm.

Table 2-1. Phenotypic comparison of p110 control and knockout mice[a]

	$\alpha^{+/+}$	$\alpha^{-/-}$	$\beta^{+/+}$	$\beta^{-/-}$
Body Weight (g)	22 ± 2	22 ± 1.6	22 ± 0.8	22 ± 1.3
% Body Fat	18.3 ± 0.2	18.6 ± 0.5	17.2 ± 0.2	16.9 ± 0.2
Liver/Body Weight	0.04 ± 0.001	0.03 ± 0.002*	0.04 ± 0.002	0.042 ± 0.003
Liver Triglyceride (mg/g)[b]	5.7 ± 0.9	4.1 ± 0.2*	5.1 ± 0.7	5.0 ± 0.2
Liver Protein (mg/g)	346 ± 53	288 ± 20	326 ± 23	312 ± 52
Liver Glycogen (mg/g)[b]	14.2 ± 0.3	5.8 ± 0.1*	13 ± 0.3	1.3 ± 0.3*
Blood Chemistry[b]				
ALT (U/L)	65 ± 19	44 ± 2	232 ± 21	156 ± 33
ALP (U/L)	85 ± 15	89 ± 10	85 ± 14	88 ± 2
Total Bilirubin (mg/dL)	0.1 ± 0.02	0.3 ± 0.01	0.2 ± 0.01	0.2 ± 0.1
Cholesterol (mg/dL)	50 ± 9	39 ± 2	74 ± 10	64 ± 5
Triglyceride (mg/dL)	50 ± 4	41 ± 4	63 ± 12	59 ± 7
Albumin (g/dL)	2.3 ± 0.1	2.1 ± 0.2	2.7 ± 0.2	2.3 ± 0.3
Total Protein (g/dL)	3.6 ± 0.3	3.3 ± 0.4	4.4 ± 0.4	3.9 ± 0.1
Glucose (mg/dL)	119 ± 2.11	118 ± 1.22	109.3 ± 4.25	150 ± 3.94*
Insulin (ng/mL)	1.96 ± 0.32	1.82 ± 0.21	0.75 ± 0.11	3.46 ± 0.53*

ALT, alanine aminotransferase; ALP, alkaline phosphatase

[a] N = 6 ; [b]Animals were fasted for 6 hours.

*p value < 0.05.

To investigate the role of PI3K isoforms in the development of HFD-induced liver steatosis, these four mouse strains were fed a diet containing 45 kcal% fat starting at 8 weeks of age. After 8 weeks on this diet, all four groups of mice gained weight (9.8 ± 0.2 g) and body fat (average increase of 42 ± 0.4% by DEXA scan). There were no significant differences in these parameters between p110-deficient animals and their $p110^{+/+}$ controls. However, ablation of p110α markedly reduced liver lipid accumulation as compared to controls as assessed by Oil Red O staining of liver sections (Fig. 2-2a). Hepatic triglyceride levels in the $p110\alpha^{-/-}$ mice were 84 ± 3% lower than in $p110\alpha^{+/+}$ mice (Fig. 2-2b). In contrast, the loss of p110β did not significantly affect liver lipid accumulation in mice fed the HFD (Fig. 2-2a and b). To determine if changes in PKCζ or Akt activity correlated with the difference in hepatic lipid content, I assayed the activity of these enzymes in liver extracts of HFD-fed mice. PKCζ activity was significantly decreased in the $p110\alpha^{-/-}$ livers as compared to $p110\alpha^{+/+}$ controls (Fig. 2-2c), but there was no significant difference in Akt activity between these two groups (Fig. 2-2d). In contrast, neither PKCζ nor Akt was affected by ablation of p110β (Fig. 2-2c and d). Thus, reduced PKCζ activity in $p110\alpha^{-/-}$ livers correlates with their resistance to HFD-induced steatosis.

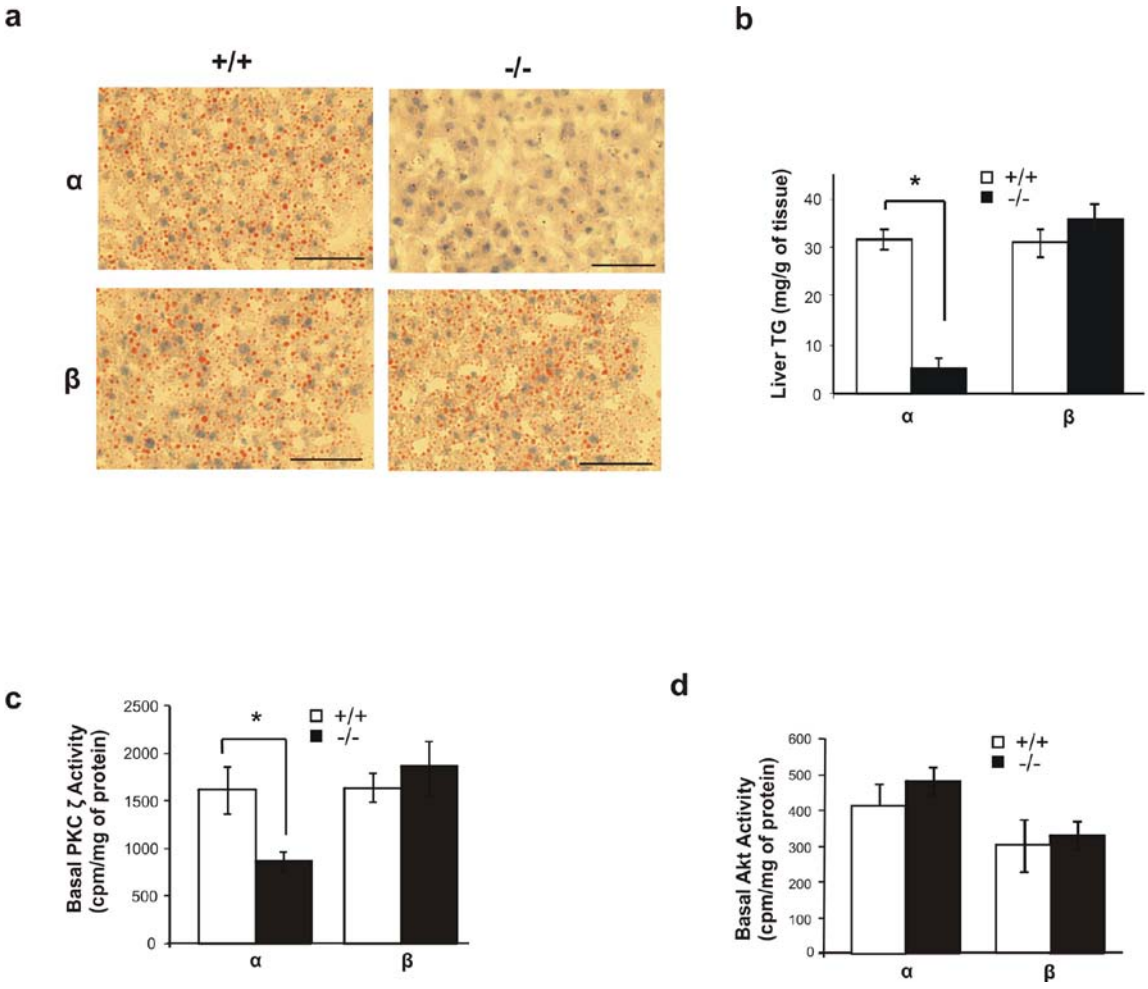

Fig. 2-2. Loss of p110α blocks hepatic steatosis induced by a high-fat diet. Mice were fed a 45 kcal% fat diet for 8 weeks. (a) Oil Red O staining of liver sections from mice of the indicated genotypes. Scale bars = 200 μm. (b) Liver triglyceride content. *$p < 0.005$ by *t*-test. N = 6. (c) Basal PKCζ kinase activity assayed in liver lysates. *$p < 0.01$ by *t*-test. N = 3. (d) Basal Akt kinase activity assayed in liver lysates. N = 3. Values are mean ± S.E.M.

2-3-2. Ablation of p110α decreases lipogenic gene expression

Previous studies have shown that expression of FAS, PPARγ and SREBP-1c is upregulated in livers of mice fed a HFD [47-48]. Using quantitative RT-PCR, I found that expression of these genes was upregulated in both $p110\alpha^{+/+}$ and $p110\alpha^{-/-}$ mice fed the HFD as compared to normal chow (Fig. 2-3a). However, with both diets the FAS and PPARγ mRNA levels were significantly lower in $p110\alpha^{-/-}$ liver than in $p110\alpha^{+/+}$ liver (Fig. 2-3a). Ablation of p110β did not affect the expression of these genes in the liver of mice on either diet (Fig. 2-3a). I next used western blotting to examine the expression level of FAS protein, a critical enzyme in fatty acid synthesis.. In mice fed normal chow, the FAS protein level was lower in $p110\alpha^{-/-}$ livers than in $p110\alpha^{+/+}$ livers (Fig. 2-3b). By contrast, hepatic FAS protein levels were similar in HFD-fed $p110\alpha^{-/-}$ and $p110\alpha^{+/+}$ mice (Fig. 2-3b). These results suggest that decreased lipogenesis may account for the lower hepatic triglyceride content in $p110\alpha^{-/-}$ mice fed normal chow (Table 2-1), but this mechanism may not be the major reason why liver triglyceride accumulation is attenuated in $p110\alpha^{-/-}$ mice fed a HFD.

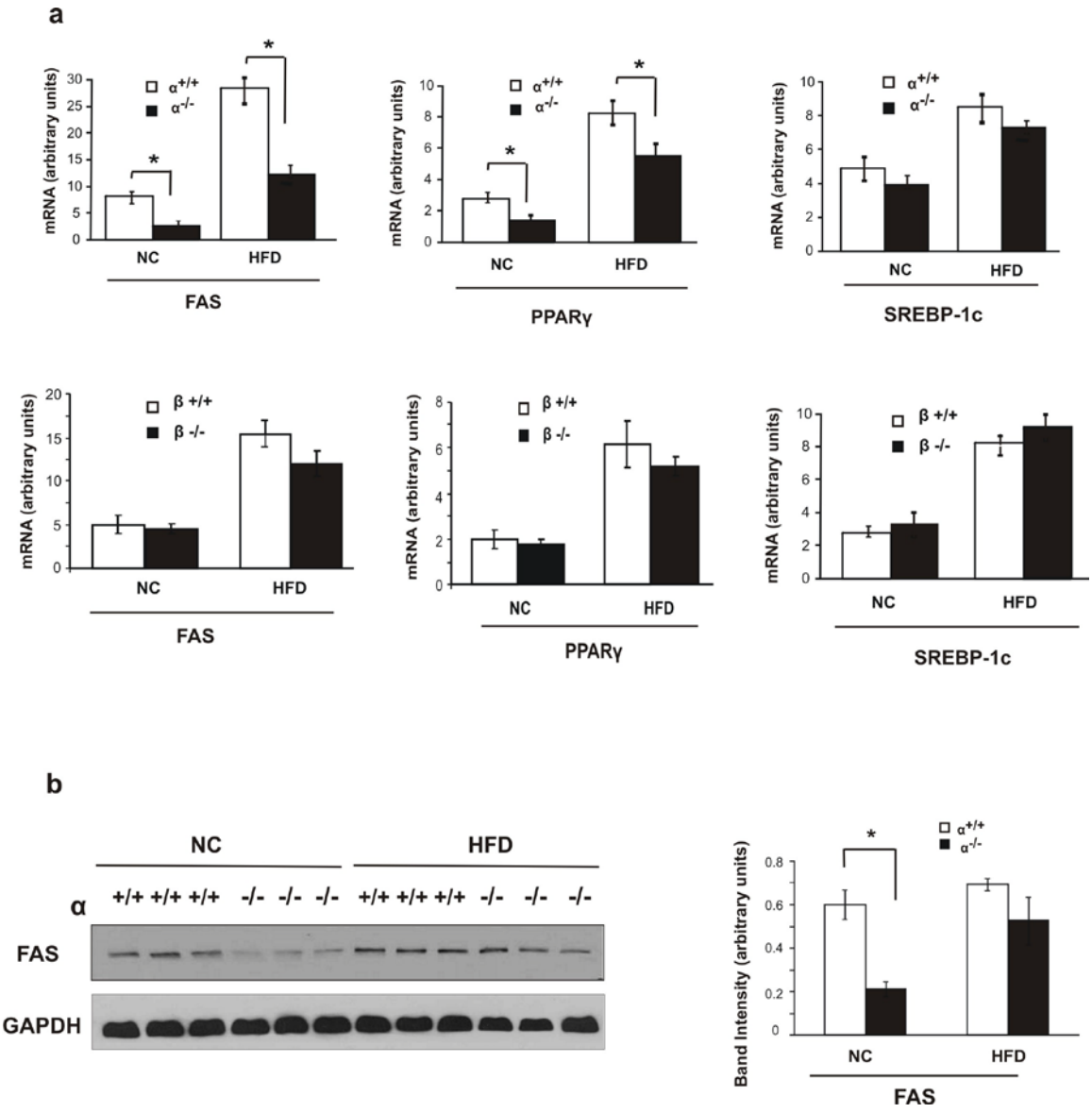

Fig. 2-3. Loss of p110α affects the expression of genes and proteins regulating lipid metabolism. (a) Quantitative RT-PCR analysis of mRNA levels in livers of mice fed a high-fat diet (HFD) or normal chow (NC). *p < 0.05 by *t*-test. N = 6. (b) Liver lysates were analyzed by western blotting with the indicated antibodies. Bands were quantified using densitometry. *p < 0.01 by *t*-test. Values are means ± S.E.M.

2-3-3. Ablation of p110α reduces hepatic fatty acid uptake

Previous studies have shown that defective uptake of long chain fatty acids (LCFA) protects mice from liver steatosis [57-59]. To determine if LCFA uptake is affected by loss of p110α in the liver, [^{3}H]palmitate uptake was assayed in hepatocytes isolated from p110α$^{+/+}$ and p110α$^{-/-}$ mice as described in Methods. I found that p110α-null hepatocytes exhibited decreased LCFA uptake as compared to p110α$^{+/+}$ control cells at most of the fatty acid concentrations tested (Fig. 2-4a). I next examined the expression of L-FABP, which regulates fatty acid uptake and metabolism in the liver and promotes the development of liver steatosis in response to a HFD [50]. Although L-FABP mRNA levels were higher in both p110α$^{+/+}$ and p110α$^{-/-}$ mice fed the HFD as compared to normal chow, the knockout livers showed lower expression than controls under both conditions (Fig. 2-4b). Liver from p110α$^{-/-}$ mice also contained decreased amounts of L-FABP protein as compared to controls; this difference was especially apparent in HFD-fed mice (Fig. 2-4c). Taken together, these results suggest that p110α$^{-/-}$ mice are protected from HFD-induced liver steatosis at least in part because of downregulation of L-FABP and decreased fatty acid uptake.

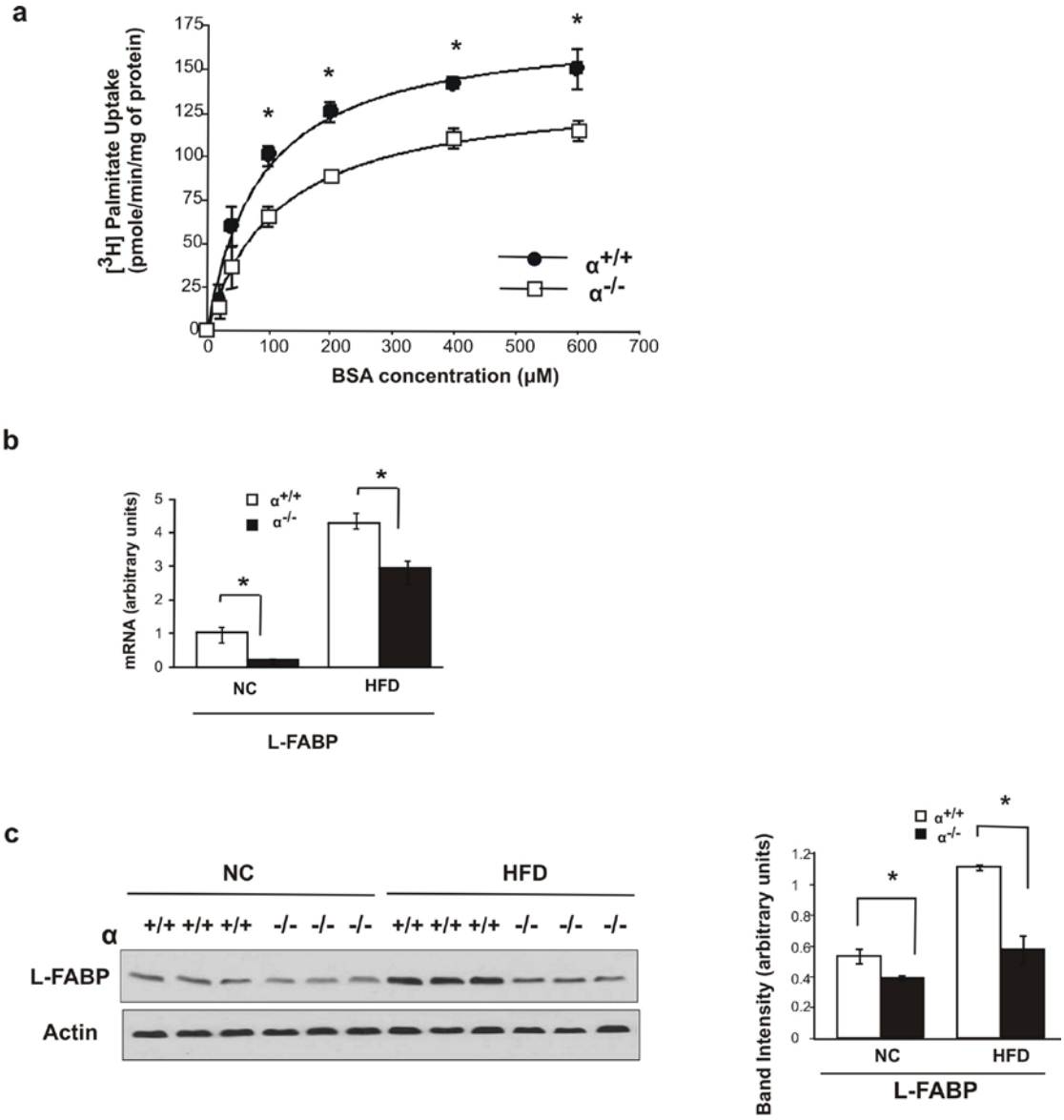

Fig. 2-4. Loss of p110α attenuates fatty acid uptake in hepatocytes. (a) Hepatocytes were isolated from p110$\alpha^{+/+}$ and p110$\alpha^{-/-}$ mice fed normal chow as described in Methods. Cells were incubated with increasing amounts of [^{3}H]oleate/BSA at a 3:1 molar ratio for 1 min. [^{3}H]oleate uptake into the cell was then measured as described in Methods. *$p < 0.001$, t-test. (b) Quantitative RT-PCR analysis of mRNA levels in livers of p110$\alpha^{+/+}$ and p110$\alpha^{-/-}$ mice fed a high-fat diet (HFD) or normal chow (NC). *$p < 0.05$ by *t*-test. N = 6. (c) Liver lysates were analyzed by western blotting with the indicated antibodies. Bands were quantified using densitometry. *$p < 0.005$ by *t*-test. Values are means ± S.E.M of three independent experiments done in triplicate.

2-3-4. Effect of PI3K ablation on HFD-induced glucose intolerance

In addition to hepatic steatosis, a HFD induces glucose intolerance in mice. Indeed, glucose tolerance tests showed that both p110α$^{+/+}$ and p110β$^{+/+}$ control mice developed this phenotype after 8 weeks on the HFD (Fig. 2-5a and 2-5b). Ablation of neither p110α nor p110β ameliorated HFD-induced glucose intolerance. In fact, p110α$^{-/-}$ mice exhibited more severe glucose intolerance than p110α$^{+/+}$ animals on the HFD (Fig. 2-5a). Similarly, HFD-induced increases in PEPCK gene expression were not inhibited by ablation of either p110α or p110β (Fig. 2-5c). Interestingly, expression of G6PC was elevated in p110α$^{-/-}$ and p110β$^{-/-}$ animals fed normal chow as compared to their controls, but no further increase in G6PC mRNA was seen in the knockout livers of mice fed the HFD (Fig. 2-5c).

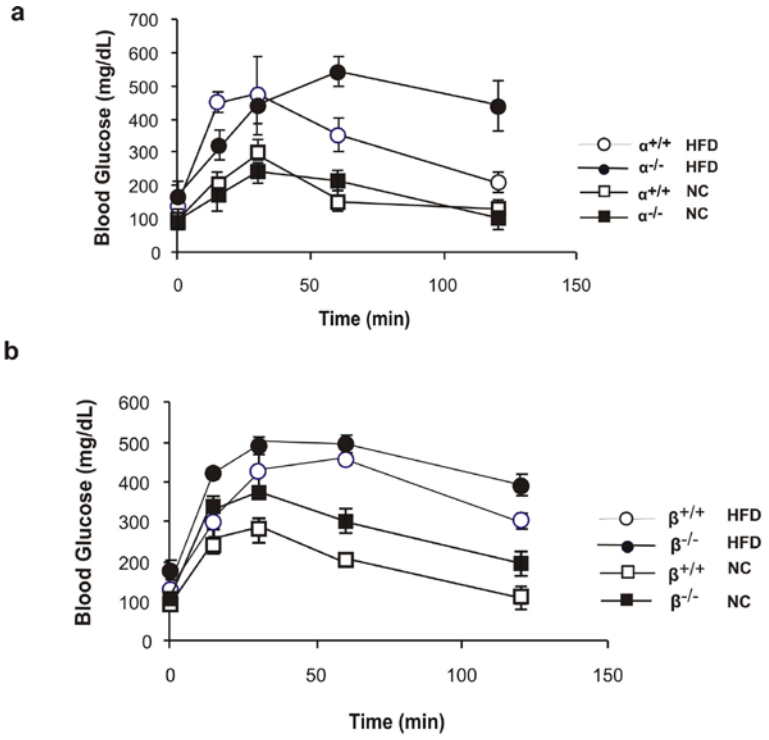

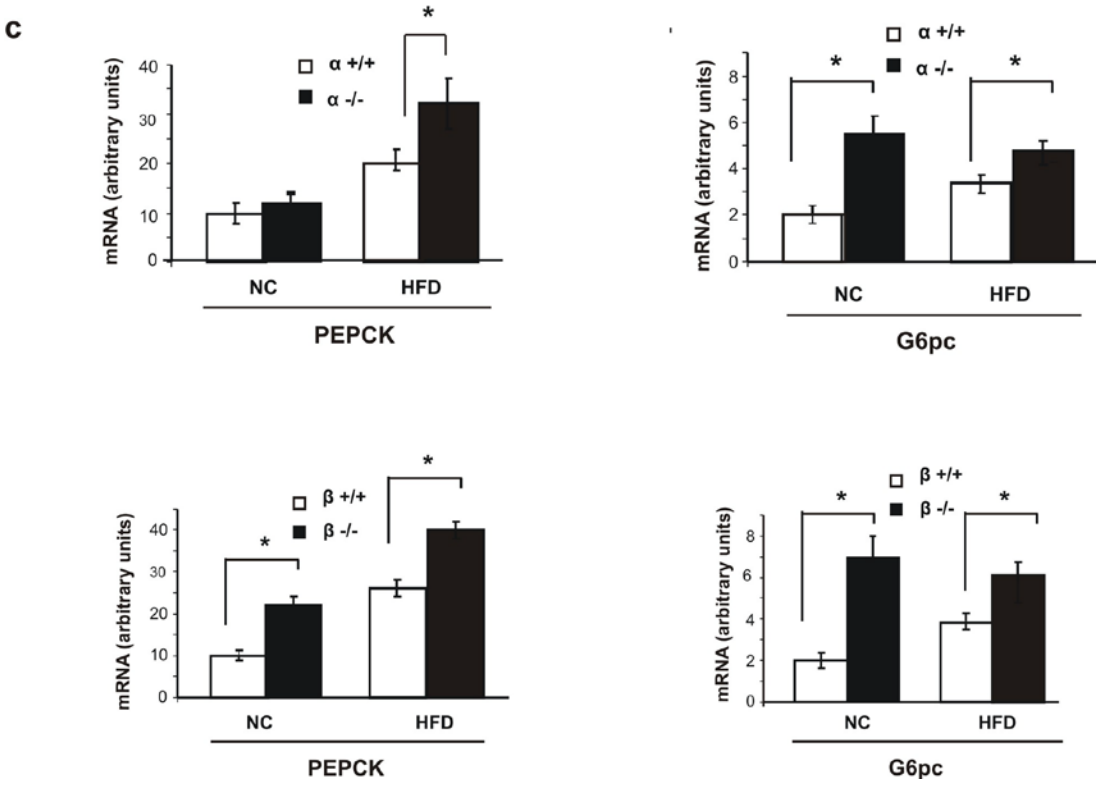

Fig. 2-5. Glucose metabolism under a high-fat diet. (a, b) Glucose tolerance tests in mice of the indicated genotypes fed a high-fat diet (HFD) or normal chow (NC). N = 6 in each group. (c) Quantitative RT-PCR analysis of mRNA levels in livers of all four strains of mice fed a high-fat diet (HFD) or normal chow (NC). *p < 0.005 by *t*-test. N = 6.

2-3-5. Ablation of p110β increases hepatic gluconeogenesis and glycogenolysis

Unlike the lipid phenotype in p110$\alpha^{-/-}$ mice, the p110$\beta^{-/-}$ mice showed defects in glucose metabolism. The p110$\beta^{-/-}$ mice (fed normal chow) exhibited elevated fasting blood glucose and insulin levels (Table 2-1) and glucose intolerance (Fig. 2-5b) as compared to p110$\beta^{+/+}$ mice. These phenotypes were not seen in the p110$\alpha^{-/-}$ animals (Table 2-1 and

Fig. 2-5a). The p110β$^{-/-}$ mice also exhibited increased expression of genes involved in glucose production in the liver (Fig. 2-5c) and elevated blood glucose production in a pyruvate challenge test (Fig. 2-6). Gluconeogenesis was not affected in the p110α$^{-/-}$ mice as measured by the same test (Fig. 2-6), although expression of G6PC was elevated in the liver of these animals (Fig. 2-5c). These phenotypes of our p110β$^{-/-}$ mice (fed normal chow) are consistent with a previous report that showed that acute deletion of p110β in the liver using adenoviral Cre resulted in animals with increased fasting blood insulin levels, glucose intolerance, and increased expression of PEPCK mRNA in the liver [60]. The p110β$^{-/-}$ mice studied by Zhao et al. [60] also produced more glucose than control animals in a pyruvate challenge test.

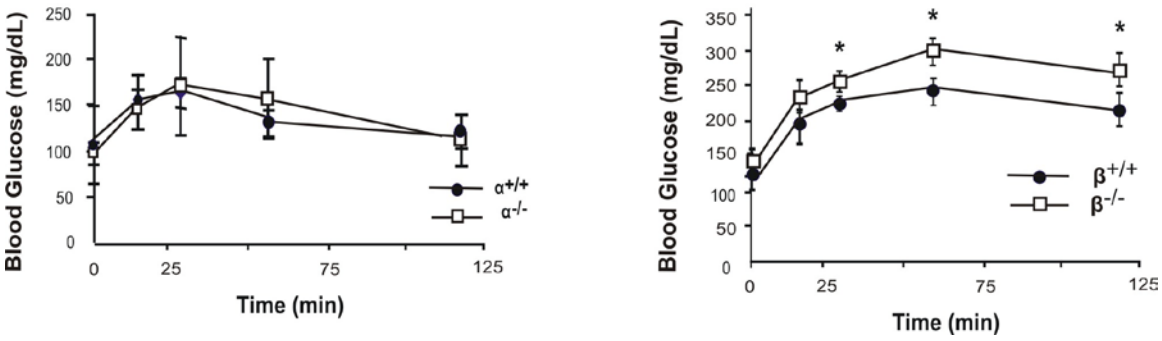

Fig. 2-6. Pyruvate challenge test. Mice were fasted overnight and injected intraperitoneally with pyruvate. Blood glucose was measured at the indicated times. *p < 0.05, *t*-test. N = 6 for each group. Values shown are mean ± S.E.M.

To avoid the involvement of other tissues besides liver that control glucose homeostasis in the whole animal, I measured the rate of gluconeogenesis in hepatocytes isolated from $p110\beta^{+/+}$ and $p110\beta^{-/-}$ mice. Cultured hepatocytes were incubated in the presence or absence of dibutyryl-cAMP and glucose levels in the medium were then assayed as described in Methods. The basal rate of gluconeogenesis was higher in $p110\beta^{-/-}$ hepatocytes than in control cells, and treatment with dibutyryl-cAMP further accentuated the difference in gluconeogenesis between knockout and control cells (Fig. 2-7a).

In addition to gluconeogenesis, breakdown of glycogen contributes to blood glucose levels. Biochemical analysis of glycogen content in livers from fasted mice showed a 90% decrease in the $p110\beta^{-/-}$ livers as compared to $p110\beta^{+/+}$ controls (Table 2-1). The glycogen content of $p110\alpha^{-/-}$ livers was also significantly reduced, but the fasting blood glucose was not elevated in these animals (Table 2-1). Periodic acid-Schiff's staining of liver sections from $p110\beta^{-/-}$ mice fasted for 6 h also revealed a dramatically lower level of glycogen as compared to the control (Fig. 2-7b). I next measured the rate of glycogenolysis in hepatocytes isolated from $p110\beta^{+/+}$ and $p110\beta^{-/-}$ mice. The basal rate of glycogenolysis was almost 2-fold higher in the $p110\beta^{-/-}$ hepatocytes than in control cells (Fig. 2-7c). As expected, dibutyryl-cAMP increased the rate of glycogenolysis in $p110\beta^{+/+}$ hepatocytes, but caused little increase in the knockout cells (Fig. 2-7c). These results suggest that increased gluconeogenesis and glycogenolysis in the liver of $p110\beta^{-/-}$ mice result in high fasting blood glucose levels, glucose intolerance and decreased liver glycogen content.

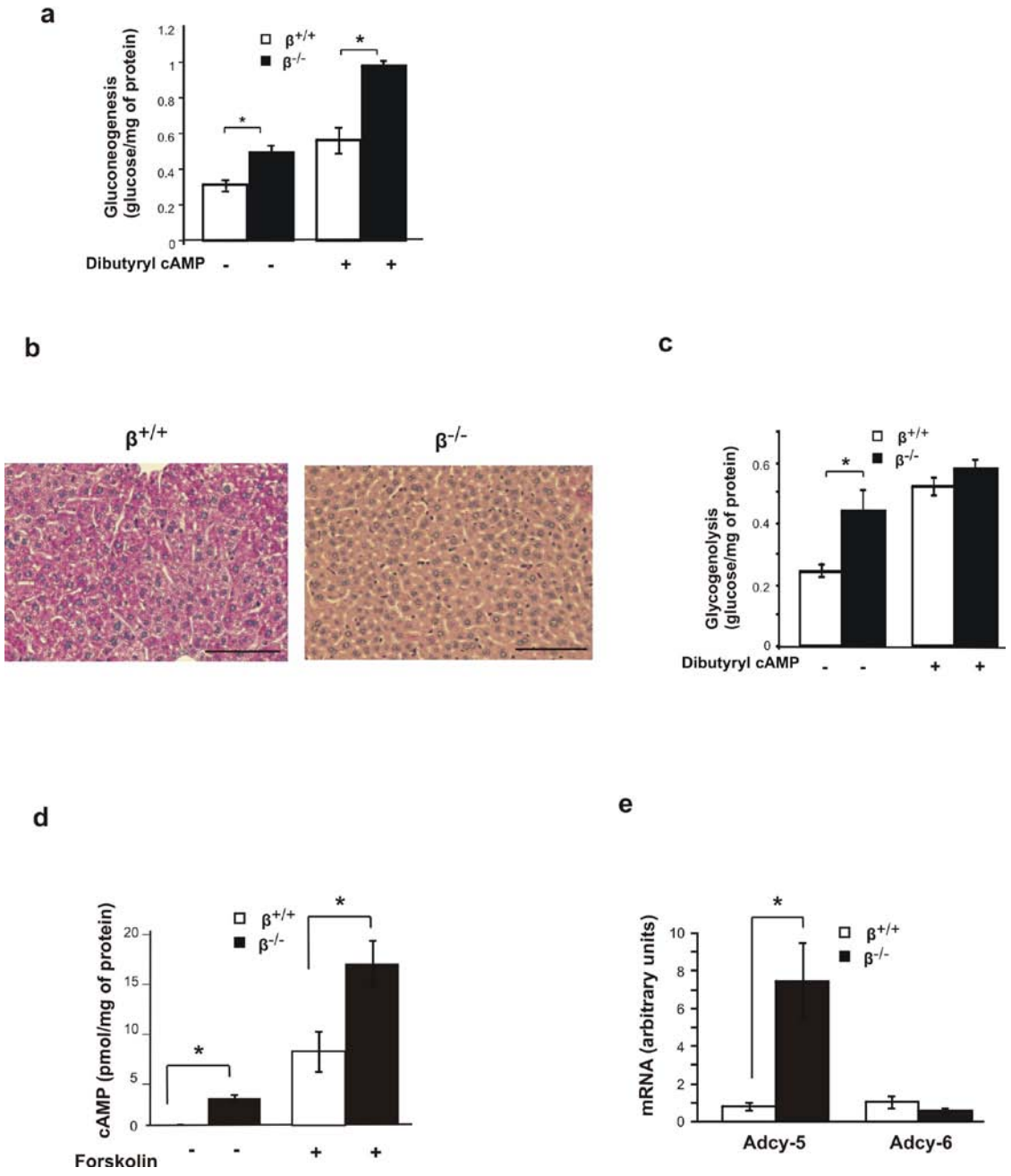

Fig. 2-7. Altered glucose metabolism and increased cAMP levels in p110β-deficient mice. (a, c) Hepatocytes were isolated from *ad lib* fed p110$\beta^{+/+}$ and p110$\beta^{-/-}$ mice. Cells were treated with or without 10 μM dibutyryl cAMP and 50 nM dexamethasone in either the absence or presence of 2 mM sodium pyruvate and 0.2 mM lactate for 5 h. Glucose production by glycogenolysis in the absence of pyruvate and lactate (c) and total glucose production in the presence of pyruvate and

lactate were measured and normalized to total protein concentration. Glucose production *via* gluconeogenesis (a) = total glucose production – glucose production by glycogenolysis. *$p < 0.05$ by *t*- test. N = 3. (b) Liver sections from $p110\beta^{+/+}$ and $p110\beta^{-/-}$ mice fasted for 6 h were stained with Periodic Acid-Schiff's Reagent. Scale bars = 200 μm. (d) cAMP levels were measured in $p110\beta^{+/+}$ and $p110\beta^{-/-}$ hepatocytes treated with or without 10 μM forskolin for 15 min. *$p < 0.001$, *t*-test. N = 3. (e) Quantitative RT-PCR analysis of mRNA levels of adenylyl cyclase 5 (Adcy-5) and adenylyl cyclase 6 (Adcy-6) in livers of $p110\beta^{+/+}$ and $p110\beta^{-/-}$ mice. *$p < 0.05$ by *t*-test. N = 6 in all groups.

2-3-6. Ablation of p110β upregulates cAMP levels in hepatocytes

Since glycogenolysis in $p110\beta^{-/-}$ hepatocytes was near maximal in the absence of exogenous cAMP (Fig. 2-7c), we wondered if these cells might have elevated levels of intracellular cAMP. Hepatocytes isolated from $p110\beta^{+/+}$ and $p110\beta^{-/-}$ mice were incubated overnight in the presence of a phosphodiesterase inhibitor prior to measuring intracellular cAMP. Under these conditions, cAMP levels were 25 times higher in $p110\beta^{-/-}$ hepatocytes than in $p110\beta^{+/+}$ cells (Fig. 2-7d). As expected, treatment with forskolin to activate adenylyl cyclase induced a significant increase in cAMP levels in both groups of hepatocytes. However, cAMP levels in forskolin-treated $p110\beta^{-/-}$ cells were still 2.2 times higher than in forskolin-treated $p110\beta^{+/+}$ hepatocytes (Fig. 2-7d). Next I examined the expression of the two most abundant adenylyl cyclase isoforms found in the liver, adenylyl cylcase 5 (Adcy-5) and adenylyl cylcase 6 (Adcy-6) [61]. Using real-time RT-PCR, I found that mRNA levels of Adcy-5 were 9 times higher in the $p110\beta^{-/-}$ livers than in $p110\beta^{+/+}$ tissue (Fig. 2-7e). The mRNA levels of Adcy-6 were not significantly different between the two groups (Fig. 2-7e). These results suggest that p110β maintains

low basal cAMP levels in hepatocytes by suppressing transcription of the Adcy-5 gene. Removal of this inhibitory mechanism in p110β-null hepatocytes could contribute to the increased gluconeogenesis and glycogenolysis exhibited by these cells.

2-3-7. Effect of PI3K ablation on insulin signaling

Attenuated insulin signaling is associated with increased hepatic glucose production and the development of liver steatosis. To investigate the effect of PI3K ablation on insulin signaling in the liver, mice were injected intraperitoneally with insulin and the livers were harvested at various times afterwards. I first used western blotting to assess the time course of Akt phosphorylation. Insulin-induced Akt phosphorylation at Ser473 was decreased in the $p110\alpha^{-/-}$ and $p110\beta^{-/-}$ livers, but phosphorylation at Thr308 was less affected (Fig. 2-8a). Insulin-stimulated phosphorylation of GSK3β and S6 was also rather indifferent to the loss of $p110\alpha^{-/-}$ or $p110\beta^{-/-}$ (Fig. 2-8a). I next assayed kinase activities in liver lysates of mice treated for 15 min with saline or hormone. Insulin activation of Akt was reduced by 49 ± 4% in the $p110\alpha^{-/-}$ livers as compared to $p110\alpha^{+/+}$ controls, whereas the activation of Akt was similar in the $p110\beta^{-/-}$ and control livers (Fig. 2-8b). Activation of PKCζ was completely blocked in the $p110\alpha^{-/-}$ liver but unaffected in the $p110\beta^{-/-}$ tissue (Fig. 2-8c).

Lastly, I measured PI3K activity in IRS-1 immunoprecipitates of liver lysates prepared from insulin-injected mice. Anesthetised mice were injected with insulin through the inferior vena cava and the livers were collected 5 min later. There was a 52 ± 6% reduction in IRS-1-associated PI3K activity in the $p110\alpha^{-/-}$ samples as compared to

the p110$\alpha^{+/+}$ controls (Fig. 2-8d), which is consistent with the decreased Akt activation in these samples (Fig. 2-8b). IRS-1-associated PI3K activity was not reduced in the p110$\beta^{-/-}$ liver lysates as compared to p110$\beta^{+/+}$ samples (Fig. 2-8d). To determine which PI3K isoform might be contributing to the residual PI3K activity observed in the p110$\alpha^{-/-}$ liver, I assayed the IRS-1 immunoprecipitates in the presence of PI3K inhibitors IC87114 (p110δ-selective), TGX-221 (p110β-selective) or PI-103 (broad spectrum). IC87114 caused a 77 ± 3% inhibition of PI3K activity in the p110$\alpha^{-/-}$ immunoprecipitate and a 51 ± 3% decrease in the p110$\alpha^{+/+}$ immunoprecipitate (Fig. 2-8d). Treatment with TGX-221 did not inhibit the PI3K activity in p110$\alpha^{-/-}$ samples, whereas PI-103 inhibited the activity by 84 ± 3% (Fig. 2-8d). Western blot analysis of liver extracts detected p110δ in the livers of all four strains of mice (Fig. 2-1a). These data suggest that a significant portion of insulin-activated PI3K activity in the liver is mediated by p110δ.

In summary, phenotypes seen in the liver-specific p110$\alpha^{-/-}$ mice may be due at least in part to attenuated insulin activation of PI3K/Akt/PKCζ signaling. On the other hand, ablation of p110β increased cAMP levels in hepatocytes without having a demonstrable effect on insulin signaling to PI3K/Akt/ PKCζ. I believe the elevated cAMP level is responsible for the increased gluconeogenesis and glycogenolysis in these knockout hepatocytes.

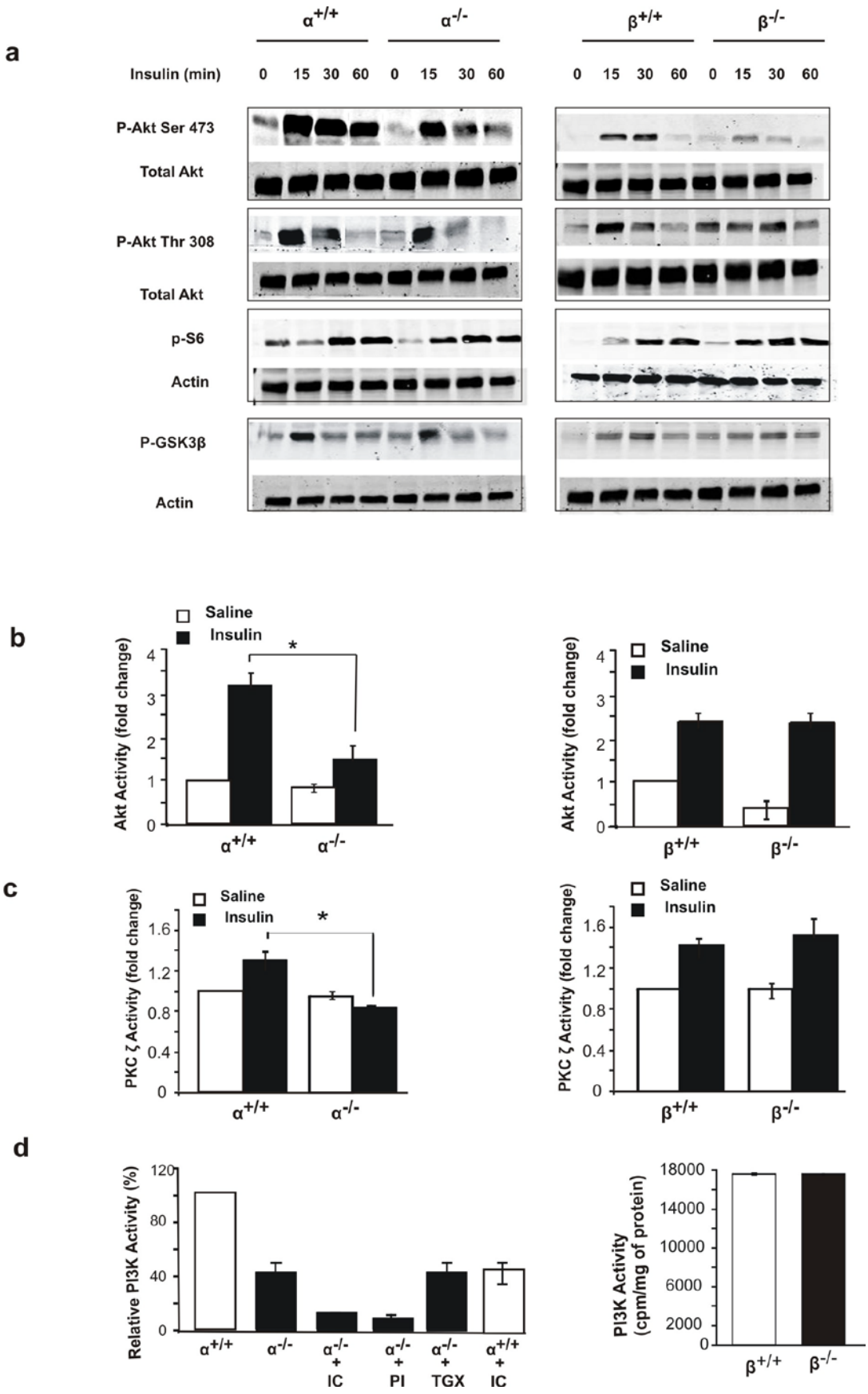
a
α+/+
α-/-
β+/+
β-/-
Insulin (min)
0 15 30 60 0 15 30 60
0 15 30 60 0 15 30 60
P-Akt Ser 473
Total Akt
P-Akt Thr 308
Total Akt
p-S6
Actin
P-GSK3β
Actin
b
Saline
Insulin
*
Akt Activity (fold change)
α+/+
α-/-
β+/+
β-/-
c
PKC ζ Activity (fold change)
d
Relative PI3K Activity (%)
α+/+
α-/-
α-/- + IC
α-/- + PI
α-/- + TGX
α+/+ + IC
PI3K Activity (cpm/mg of protein)

Fig. 2-8. **Insulin signaling in p110β-null livers.** (a) Liver lysates from fasted mice treated intraperitoneally without or with insulin (2 U/kg body weight) for the indicated times were analyzed by western blotting. (b, c) Fasted mice were injected intraperitoneally with saline or insulin (2 U/kg body weight). Livers were collected 15 min later and lysates were prepared and assayed for Akt or PKCζ kinase activity. *p <0.05 by *t*-test. N = 3 for all groups. (d) All four strains of mice were fasted overnight and then injected through the inferior vena cava with insulin (2 U/kg body weight). Livers were collected 5 min later and lysates were prepared and subjected to immunoprecipitation with IRS-1 antibody. The immunoprecipitates for $p110\alpha^{+/+}$ and $p110\alpha^{-/-}$ were assayed for PI3K activity in the presence of 500 nM PI-103 (PI), 50 nM TGX-221 (TGX), 5 μM IC87114 (IC) or vehicle. Values are normalized to the average PI3K activity in $p110\alpha^{+/+}$ samples assayed in the absence of inhibitors. The immunoprecipitates for $p110\beta^{+/+}$ and $p110\beta^{-/-}$ were assayed for PI3K activity. N = 3 for all groups. Values shown are mean ± S.E.M.

2-4. DISCUSSION

Previous studies using various mouse models and pharmacological compounds have shown the importance of PI3Ks in regulating hepatic glucose and lipid metabolism under normal physiological conditions [40, 60]. However, the roles of PI3K isoforms in the development of HFD-induced fatty liver and glucose intolerance are unknown. To address this, I studied liver-specific p110α or p110β knockout mice fed a HFD and found that ablation of p110α but not p110β blocked liver steatosis. Surprisingly, I found that the loss p110α reduced fatty acid uptake into hepatocytes and decreased basal L-FABP expression and its upregulation induced by HFD feeding. Another surprising finding from my study is that the basal cAMP levels were elevated in the p110β-null hepatocytes. This probably is due to increased expression of Adcy-5 in these cells. An increased cAMP level is probably the reason why the rates of gluconeogensis and glycogenolysis are elevated in the p110β-null hepatocytes, leading to hyperglycemia and glucose intolerance in the animals.

Although increased lipid synthesis under conditions of a HFD seems counterintuitive, increased *de novo* lipogenesis has been shown to contribute to the triglyceride content of steatotic livers of obese patients [62]. I found that induction of FAS and PPARγ mRNA was significantly reduced in the $p110\alpha^{-/-}$ liver. Decreased PKCζ activity in the liver of HFD-fed $p110\alpha^{-/-}$ mice is one possible explanation for reduced expression of lipogenic genes and protection from HFD-induced liver steatosis. Inhibition of hepatic aPKC by adenoviral expression of a dominant negative kinase-dead PKCζ

mutant diminished diet-induced increases in SREBP-1c mRNA and improved hepatosteatosis in mice fed a HFD [63].

On the other hand, a number of recent studies have questioned the importance of upregulated lipogenesis in diet-induced liver steatosis. For example, liver-specific knockout of acetyl-CoA carboxylase 1, another critical lipogenic enzyme, did not protect mice from the development of HFD-induced fatty liver [64], and a relative decrease in the contribution of *de novo* lipogenesis to hepatic triglyceride was reported in rats fed a HFD [65]. Another study concluded that lipid accumulation in the liver of HFD-fed mice is due to adaptive remodeling of hepatic fatty acids due to increased fatty acid influx rather than increased *de novo* lipogenesis [66]. My result showing that the FAS protein level was not significantly upregulated in the liver of HFD-fed control mice also questions the importance of upregulated lipogenesis in diet-induced liver steatosis. In addition, HFD induced a large increase in the amount of FAS protein in the $p110\alpha^{-/-}$ livers, even though they were protected from steatosis. Thus, ablation of p110α did not seem to block HFD-induced liver steatosis by inhibiting lipogenesis. Ablation of $Akt2^{-/-}$ also blocked HFD-induced liver steatosis without inhibiting lipogenesis [49]. However, my HFD-fed $p110\alpha^{-/-}$ mice did not exhibit decreased Akt activity in the liver. In contrast to the HFD condition, the hepatic FAS protein level in $p110\alpha^{-/-}$ mice fed normal chow was significantly lower than in control mice, as was the hepatic triglyceride content. These results suggest that p110α might promote lipid synthesis in the liver under normal dietary conditions by regulating FAS gene expression.

Another source of triglycerides in the liver is uptake of fatty acids from the blood. It was estimated that about 70% of the triglyceride fatty acids in the liver of patients with

hepatic steatosis comes from serum non-esterified fatty acids plus dietary fatty acids [62]. Estimates of endogenous hepatic fatty acid binding activity [67] suggested that L-FABP is likely the most important fatty acid binding protein in the mammalian liver. *In vitro* studies demonstrated increased fatty acid uptake in cells with upregulated expression of L-FABP [68-69], and L-FABP knockout mice showed altered fatty acid uptake and decreased hepatic triglyceride [70]. It was shown that expression of L-FABP can be upregulated by a HFD and loss of L-FABP protects mice from HFD-induced hepatic steatosis [71]. I found that ablation of p110α essentially blocked the increase in L-FABP protein levels in mice fed the HFD. In addition, fatty acid uptake was significantly decreased in $p110\alpha^{-/-}$ hepatocytes. My results suggest that reduced fatty acid uptake as a consequence of decreased L-FABP expression is an important mechanism that protects $p110\alpha^{-/-}$ mice from HFD-induced liver steatosis. The regulation of L-FABP gene expression is not well understood, but there is some evidence that PPARα plays a role in its activation [72]. Interestingly, I found that the PPARα mRNA level was decreased in the $p110\alpha^{-/-}$ liver (data not shown). Additional studies are needed to identify the mechanisms by which p110α regulates L-FABP expression.

Hepatic steatosis is closely associated with glucose intolerance. However, ablation of neither p110α nor p110β attenuated glucose intolerance induced by the HFD. In fact, glucose intolerance in $p110\alpha^{-/-}$ mice was worse than in the HFD-fed controls. Upregulation of the PEPCK gene in the p110α knockout mice might contribute to this phenotype. Surprisingly, ablation of p110β resulted in higher fasting glucose and insulin levels in mice fed normal chow. Hyperglycemia in these animals is most likely due to an increased level of cAMP in the $p110\beta^{-/-}$ hepatocytes that upregulates gluconeogenesis and

glycogenolysis. Although hyperglycemia and hyperinsulinemia can result from insulin resistance, I found that insulin signaling to PI3K, Akt and PKCζ was essentially intact in the p110β-null liver. Insulin-induced phosphorylation of Akt at Ser473 was reduced in the $p110\beta^{-/-}$ liver, but Akt activity was not decreased. This is consistent with the current understanding that Thr308 is the major site that regulates Akt activity [73].

The role of cAMP in liver physiology has been studied extensively. Increased production of cAMP in hepatocytes in response to glucagon leads to CREB (cAMP responsive element binding) phosphorylation and activation of gluconeogenesis and glycogenolysis. Abnormal cAMP levels in the liver cause defects in glucose metabolism. For example, mice with low cAMP levels due to decreased β-adrenergic receptor density exhibited reduced PEPCK and G6PC mRNA and protein levels [74]. On the other hand, higher cAMP levels due to overexpression of the β_2-adrenergic receptor in the liver increased PEPCK and G6PC gene expression and reduced the glycogen content [75]. Recent studies showed that the class IB PI3K p110γ suppresses cAMP levels in the heart by binding to and activating phosphodiesterase PDE3B [76-77]. Here I found that hepatocytes isolated from $p110\beta^{-/-}$ liver exhibited high intracellular cAMP levels and upregulated expression of Adcy-5. Whole-body knockout and heart-specific overexpression of Adcy-5 have elucidated its roles in cardiac contractility and motor coordination [78-80], but its function in the liver is not known. My data strongly suggest that p110β suppresses Adcy-5 transcription in the liver. To my knowledge, this is the first report showing that a class IA PI3K can regulate cAMP. Further studies are needed to define the mechanism of regulation involved in this process.

Activation of PI3K signaling controls many aspects of the insulin-mediated regulation of glucose metabolism. Although insulin activation of PI3K and Akt were both attenuated in the p110$\alpha^{-/-}$ liver, these effects did not lead to hyperglycemia in the animal. I suspect that this is due to the residual Akt activation observed in the knockout liver, which is adequate to signal downstream. Indeed, insulin-stimulated phosphorylation of GSK3β and S6 were both unaffected in the p110$\alpha^{-/-}$ liver (Fig. 2-5c). The residual Akt activation seems to be due to recruitment of p110δ into the IRS-1 complex following insulin stimulation. Although p110δ is believed to be expressed mostly in immune cells, I detected it in mouse liver. Future studies using p110δ knockout mice will help clarify the role of this PI3K isoform in regulating hepatic metabolic processes.

In conclusion, the data presented here indicate that p110α but not p110β plays a pivotal role in the development of liver steatosis induced by HFD feeding. The mechanism of reduced lipid accumulation in the p110$\alpha^{-/-}$ liver is likely due to lower fatty acid uptake resulting from decreased expression of L-FABP. My study also revealed a novel interaction between p110β and cAMP signaling that could explain why the p110$\beta^{-/-}$ mice have increased hepatic gluconeogenesis and glyogenolysis leading to glucose intolerance. Since fatty liver disease and glucose intolerance pose epidemic problems for public health, a better understanding of the pathways that regulate lipid accumulation and glucose regulation in the liver is crucial for developing effective therapies for these conditions.

Chapter 3.

$G\alpha_q$ Binds to p110α/p85α PI3K and Displaces Ras

3-1. INTRODUCTION

GPCRs transduce a wide variety of extracellular stimuli including light, neurotransmitters, odorants, hormones, nucleotides, chemokines and many others into intracellular signals that regulate a large number of cellular processes. The specific intracellular effector that is modulated upon receptor activation depends on which subtype of G protein subunit couples to the receptor. In response to $G\alpha_q$-coupled receptor activation, the canonical signaling molecule activated by $G\alpha_q$ is PLCβ [81-82]. However, our laboratory and others have found that activation of $G\alpha_q$-coupled receptors can also lead to inhibition of the PI3K/Akt signaling pathway [52]. In subsequent studies, our laboratory found that the inhibitory effect of $G\alpha_q$ on PI3K signaling is independent of PLCβ activation [37, 83].

Based on these results, I hypothesized that $G\alpha_q$ binds directly to the PI3K complex to inhibit its activity. In this chapter, I used purified recombinant proteins to measure $G\alpha_q$ binding to p110α/p85α using fluorescence spectroscopy and examined the effect of $G\alpha_q$ on the lipid kinase activity of various PI3K isoforms *in vitro*. Lastly, I also examined the effect of $G\alpha_q$ on binding of activated Ras to PI3K. Results from these studies indicate that activation of $G\alpha_q$ can directly inhibit PI3Ks, suggesting that these enzymes represent a new class of signaling effector of $G\alpha_q$.

3-2. MATERIALS AND METHODS

Materials

HA (haemagglutinin) antibody was obtained from Covance (Richmond, CA, U.S.A.). FLAG antibody was from Sigma (St. Louis, MO, U.S.A.). Phospho-Ser217/Ser221 MEK1/2 antibody (MEK is mitogen-activated protein kinase/extracellular signal-regulated kinase kinase) was obtained from New England Biolabs (Beverly, MA, U.S.A.). Recombinant p110γ protein was purchased from Axxora (San Diego, CA, U.S.A.).

Constructs and recombinant proteins

The cDNA for human H-Ras was obtained by RT-PCR from HEK-293 (human embryonic kidney 293) cell RNA. It was used as a template to make V12Ras by PCR-based mutagenesis. The cDNA for histadine tagged K-RasQ12V-4B (KRas) was obtained from Dr. Nicolas Nassar. Bacterial cells were transformed and recombinant K-Ras was purified using Ni-NTA agarose and gel filtration column. GST-Raf1-RBD was purified from bacterial cells and the K-Ras protein was confirmed to be functional and active by its interaction with the Raf1-RBD. Purified recombinant H-Ras (amino acids 1–166) expressed in *Escherichia coli* was generously provided by Dr N. Nassar (Stony Brook University, Stony Brook, NY, U.S.A.).

To make GST (glutathione S-transferase)–p110α fusion proteins, fragments encompassing the various p110α domains were made by PCR and then subcloned into pGEX-5X-3 (Amersham Biosciences, Piscataway, NJ, U.S.A.). GST and the GST–p110α

fusion proteins were expressed in *E. coli* and purified using glutathione–Sepharose 4B (Amersham Biosciences).

FLAG–p110α was described previously [37]. FLAG–p110α amino acids 1–116 were made by mutating codon 117 of p110α to a stop codon. p110α amino acids 118–1068 were made by PCR using p110α as a template and the fragment was then subcloned into p3XFLAG-CMV10 (Sigma) to make FLAG–p110α amino acids 118–1068. FLAG–p110γ was constructed by subcloning the p110γ insert of IMAGE clone number 5749986 into p3XFLAG-CMV10. HA–$G\alpha_q$Q209L and $G\alpha_q$Q209L were described previously [37, 83]. FLAG–p85α mutants (muts) were made by PCR using p85α as a template and the fragments were then subcloned into p3XFLAG-CMV10 to make FLAG-p65 (amino acids 1-572), FLAG-mut. 1 (1-498), FLAG-mut. 2 (1-514), FLAG-mut. 3 (1-520), FLAG-mut. 4 (1-546) and FLAG-nSH2 (1-490). HA–MEK1 was a gift from N. G. Ahn (University of Colorado, Boulder, CO, U.S.A.). Akt–HA was obtained from R. Roth (Stanford University, Stanford, CA, U.S.A.).

Purification of the p110α/p85α PI3K complex [37] and $G\alpha_q$ [84] from baculovirus-infected Sf9 cells was described previously. Briefly, mouse genes for the expression of PI3K Class IA subunits were cloned by PCR from mouse liver cDNA. Using homologous recombination, the p110α and p110β subunits were subcloned into N-terminal His tagged insect cell expression vector, and the p85α and p85β subunits were subcloned into untagged insect cell expression vector. Sf9 cells were cotransfected with the plasmid and linear viral DNA and a baculovirus clone expressing the recombinant protein was isolated. The baculovirus was further purified by plaque assay. To make the recombinant PI3K p110/p85 complex, Sf9 cells were infected with different

combinations of His tagged-p110 (α or β) and p85 (α or β) baculoviruses. The protein was purified by passing it through a QFF (anion exchange column) and a Ni-NTA column. Purified recombinant PI3K complexes were detected by coomassie stain of SDS-PAGE analysis as well as immunoblotting with specific PI3K catalytic and regulatory subunit antibodies.

The recombinant $G\alpha_q$ was purified from Sf9 insect cells infected with baculovirus encoding $G\alpha_q$ and the $\beta_1\gamma_2$-HIS tagged heterodimer. Following the preparation of plasma membranes containing the G protein subunits, the protein was extracted from the membrane using detergent. The purification of $G\alpha_q$ was based on the method of attaching the heterotrimer to Ni-NTA sepharose through the HIS tag on the γ_2 subunit, and subsequent separation of $G\alpha_q$ from the $\beta_1\gamma_2$ dimer by its activation. The $G\alpha_q$ protein was further purified by passing it through an anion exchange column (mono Q column).

Cell culture, lysate preparation and immunoprecipitation

HEK-293 cells and COS7 cells were maintained in Dulbecco's modified Eagle's medium (Sigma) containing 10% (v/v) fetal bovine serum (Sigma) and antibiotics. COS7 cells were transfected using Lipofectamine™ (Invitrogen, Carlsbad, CA, U.S.A.). HEK-293 cells were transfected using TransIT-293 (Mirus, Madison, WI, U.S.A.) following standard methods. The FreeStyle 293 Expression System (Invitrogen) was used to express HA–$G\alpha_q$Q209L.

Cells were rinsed with ice-cold PBS 2 days after transfection and scraped into lysis buffer (50 mM Hepes, pH 7.5, 50 mM NaCl, 5 mM EDTA, 50 mM NaF, 10 mM sodium pyrophosphate, 1 mM sodium orthovanadate, 0.5 mM PMSF and 10 μg/ml

aprotinin and leupeptin) with either 1% Triton X-100 or 1% Nonidet P40 plus 0.25% sodium deoxycholate. Homogenates were centrifuged at 15000 *g* for 15 min at 4 °C, and protein concentrations of the supernatants were determined using a Bradford assay (Bio-Rad, Hercules, CA, U.S.A.).

Cell lysates containing equal amounts of protein were incubated with the appropriate antibody for 2 h and then with 25 μl of protein A- or protein G-agarose (Sigma) for 1 h. The beads were either washed three times with lysis buffer and used for immunoblotting or washed three times with the appropriate kinase assay buffer prior to performing kinase assays.

Kinase assays and western blots

Akt activity was assayed following a method described previously [52]. PI3K was assayed as described previously [52] except that the PI3K assay buffer contained 40 mM Hepes (pH 7.5), 1 mg/ml fatty acid-free BSA, 2 mM EGTA and 100 mM NaCl. Western blot signals were visualized using horseradish peroxidase-linked secondary antibodies (Amersham Biosciences) and chemiluminescence reagents (PerkinElmer Life Sciences, Boston, MA, U.S.A.) [52].

Fluorescence measurements and data analysis

Purified $G\alpha_q$ was stored in a solution containing 20 mM Hepes (pH 7.2), 1 mM EDTA, 3 mM $MgCl_2$, 400 mM NaCl, 0.7% CHAPS and 50 μM GDP (GDP buffer). To activate $G\alpha_q$, the protein was incubated for 1 h at 30 °C in GTP[S] (guanosine 5′-[γ-thio]triphosphate) buffer (50 mM Hepes, pH 7.2, 100 mM $(NH_4)_2SO_4$, 150 mM $MgSO_4$,

1 mM EDTA, 0.7% CHAPS and 100 μM GTP[S]) [85]. To activate Ras, the protein was incubated in a buffer containing 20 mM Hepes (pH 7.2), 200 μM $(NH_4)_2SO_4$, 5 mM EDTA and 5 μM GTP[S] for 1 h on ice. The reaction was stopped by adding 20 mM $MgSO_4$ and the protein was dialyzed against buffer A (20 mM Hepes and 160 mM KCl, pH 7.2) plus 1 mM 2-mercaptoethanol for 30 min.

Prior to labeling with 7-(dimethylamino) coumarin-4-acetic acid succinimidyl ester (referred to as coumarin; Molecular Probes, Eugene, OR, U.S.A.), both $G\alpha_q$ and Ras were dialyzed overnight against buffer A. The pH of the $G\alpha_q$ and Ras solutions was raised by adding 1 μl of 2 M K_2HPO_4 (pH 8.5) per 100 μl before labeling with a 4-fold molar excess of coumarin. The reaction mixtures were incubated on ice for 1 h and then free probe was removed by dialysis against buffer A at 4 °C.

LUVs (large unilamellar vesicles), 0.1 μm in diameter, were formed from a 2:1 mixture of POPC (1-palmitoyl-2-oleoyl phosphatidylcholine) and PS (1-palmitoyl-2-oleoyl-*sn*-glycero-3-phospho-L-serine; Avanti Polar Lipids, Alabaster, AL, U.S.A.). Lipids were dissolved in chloroform, dried under vacuum and resuspended in buffer A at room temperature (22 °C). The lipids were then subjected to five cycles of freeze–thawing to form multilamellar vesicles and then extruded through a polycarbonate filter (0.1 μm diameter) for ten cycles to produce LUVs.

Fluorescence measurements were performed on an ISS spectrofluorimeter (ISS, Champaign, IL, U.S.A.) in 3 mm pathlength cuvettes that were filled with 120 μl of sample. All samples contained 80 μM LUVs. Buffer controls used buffer A plus 1 mM dithiothreitol. Coumarin-labeled proteins were excited at 340 nm and fluorescence emission intensity was scanned from 380 to 580 nm. The integrated area was calculated

for each point of the titration curve. Binding to either coumarin–$G\alpha_q$ or coumarin–Ras resulted in a maximal 20% increase in fluorescence. The spectra were corrected for loss of fluorescence caused by dilution from addition of buffer alone. These background-corrected spectra were then normalized to the last point on the titration curve to give a final value of 1.0. This process assumes complete binding and allows us to determine apparent dissociation constants (K_d) in nanomolar units when the data are fitted to a bimolecular association curve. Experiments were performed in triplicate and results shown are the means±S.E.M.

3-3. RESULTS

3-3-1. Activated $G\alpha_q$ interacts with PI3K complexes *in vivo*

Binding of activated $G\alpha_q$ to PI3K isoforms was first tested in cells. COS7 cells were cotransfected with various FLAG epitope-tagged p110 and p85 complexes (p110α/p85α, p110α/p85β, p110β/p85α, and p110β/p85β) in the presence or absence of HA epitope-tagged $G\alpha_q$Q209L. The constitutively active $G\alpha_q$Q209L mutant is bound to GTP and thus circumvents the need for receptor activation. Cell lysate proteins were immunoprecipitated with HA antibody and the immunoprecipitates were analyzed by western blotting with a FLAG antibody. All four FLAG-p110/p85 complexes were detected in the HA-$G\alpha_q$Q209L immunoprecipitates (Fig. 3-1). The blot was reprobed with the HA antibody to confirm the presence of HA-$G\alpha_q$Q209L. The expression of FLAG-p110s was also confirmed by analyzing the cell lysates by western blotting using the FLAG antibody (Fig. 3-1). These results suggest that activated $G\alpha_q$ can bind to all four PI3K p110/p85 complexes tested.

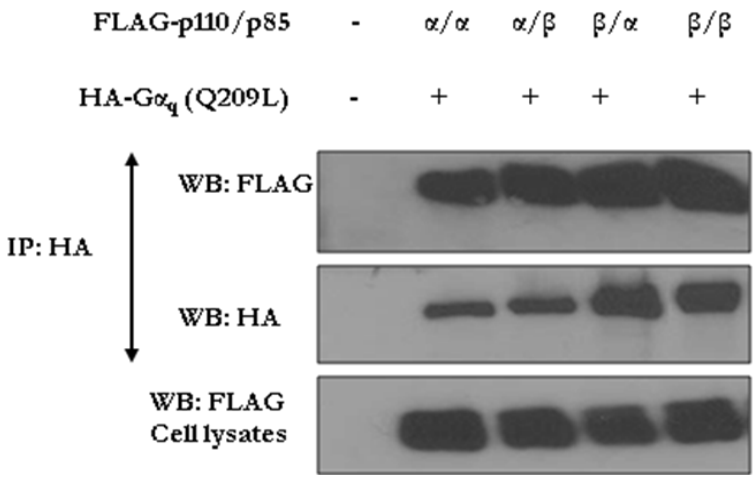

Fig. 3-1. Co-immunoprecipitation of GαqQ209L with PI3K isoforms. COS7 cells were transfected with FLAG-p110 and p85 isoforms to produce complexes p110α/p85α, p110α/p85β, p110β/p85α, or p110β/p85β (α/α, α/β, β/α, or β/β respectively) and with HA-$G\alpha_q$Q209L. Immunoprecipitation (IP) with HA antibody followed by western blotting (WB) with anti-FLAG antibody detected the presence of p110/p85 complexes (top panel). The blot was reprobed with anti-HA antibody to confirm the presence of HA- $G\alpha_q$Q209L (middle panel) in the immunoprecipitates. Western blot analysis of cell lysate proteins with FLAG antibody confirmed the expression of PI3K complexes (bottom panel).

3-3-2. $G\alpha_q$ inhibits lipid kinase activity of PI3K isoforms

To test if a direct interaction between $G\alpha_q$ and p110/p85 affects lipid kinase activity, $G\alpha_q$ and the PI3K complexes p110α/p85α, p110α/p85β, p110β/p85α and p110β/p85β were purified from baculovirus-infected Sf9 cells as described in Methods. First, the lipid kinase activity of the various PI3K isoforms in the absence of $G\alpha_q$ was determined using *in vitro* PI3K activity assays with PI as a substrate. The reaction was started by adding [γ^{32}P]ATP. The reaction product was separated by thin layer chromatography (TLC) and counted in a scintillation counter. Specific activity for each isoform was calculated from the counts obtained. These data show that the PI3K p110α isoforms were the most active, having more than ten times higher activity than the p110β isoforms (Fig. 3-2A). The relative specific activities of the four isoforms were p110α/p85α ≥ p110α /p85β >> p110β/p85β > p110β/p85α.

Next, the purified PI3K proteins were tested to see if $G\alpha_q$ inhibits their lipid kinase activity *in vitro*. $G\alpha_q$ was activated with GTP[S], incubated with the PI3K complexes and then PI3K assays were performed. Addition of $G\alpha_q$·GTP[S] inhibited p110β/p85β activity by 99.3 ± 5.2% and p110β/p85α activity by 79.7 ± 31.7% (Fig. 3-2B). To a lesser extent, $G\alpha_q$·GTP[S] also inhibited p110α/p85β (65.8 ± 9.3%) and p110α/p85α (36 ± 4.7%) (Fig. 3-2B). These results show that activated $G\alpha_q$ directly inhibits all four PI3K complexes *in vitro* but with varying intensities.

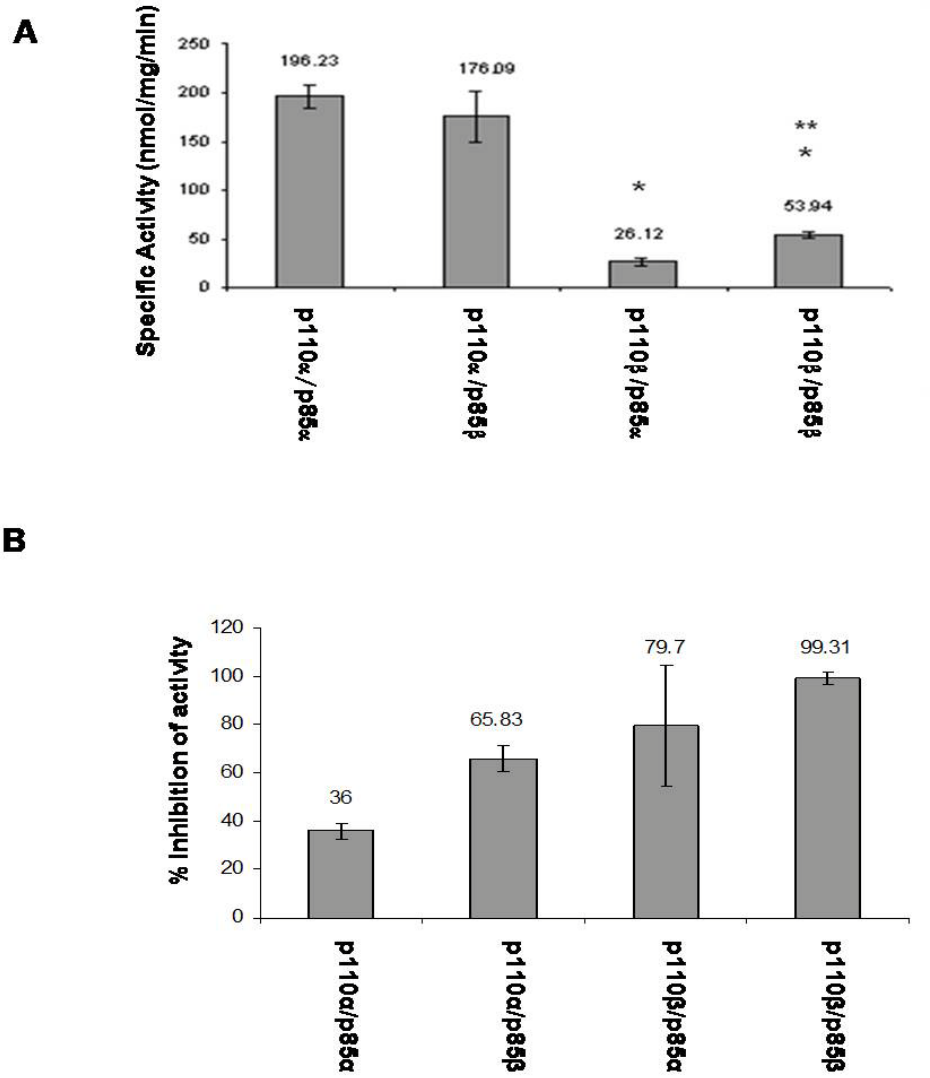

Fig. 3-2. Effect of $G\alpha_q$ on the activity of PI3K isoforms. (A) Specific activity of purified PI3K complexes was assayed *in vitro* by detecting production of [^{32}P]PI(3)P from PI and [γ^{32}P]ATP. The lipids were separated on TLC plates. *$p < 0.001$ by one way ANOVA with post hoc tukey test between the p110β and p110α isoforms. **$p < 0.01$ by *t*-test between p110β/p85α and p110β/p85β. (B) $G\alpha_q$·GTP[S] or activation buffer (control) was mixed with or without (blank) an equal concentration of purified PI3K complex. *In vitro* PI3K assays were performed, radioactivity in [^{32}P]PI(3)P was counted, and % inhibition of PI3K activity by $G\alpha_q$·GTP[S] was calculated for each complex. N = 3 for each group. Values are mean ± S.E.M.

3-3-3. $G\alpha_q$ directly binds to p110α/p85α *in vitro*

Next, I used fluorescence spectroscopy as another technique to test if there is a direct protein-protein interaction between $G\alpha_q$ and PI3K. $G\alpha_q$ was activated with GTP[S], labeled with coumarin and reconstituted into lipid vesicles. Increasing concentrations of PI3K proteins were then titrated into the solution. The emission intensity of the coumarin-labeled $G\alpha_q$, which increases upon binding to other proteins [86], was then measured. Coumarin labeling does not impair $G\alpha_q$ function, since coumarin–$G\alpha_q$ activates PLCβ enzymes as efficiently as unlabeled $G\alpha_q$ [86]. Fig. 3-3 shows that addition of increasing amounts of p110α/p85α PI3K into a solution containing active $G\alpha_q$·GTP[S] caused an increase in fluorescence that reached a plateau at approx. 100 nM PI3K. The dissociation constant, K_d, was calculated to be 11 ± 1 nM when the data were fit to a bimolecular association curve (Fig. 3-3). By comparison, K_d values for coumarin-labeled $G\alpha_q$·GTP[S] binding to three isotypes of PLCβ ranged from 0.3 to 2.8 nM, as determined by fluorescence resonance energy transfer (data in [86]were recalculated to give K_d

values at the same lipid concentration used in these studies). The increase in fluorescence was reversed when trypsin was added to the solution (results not shown). The K_d for inactive $G\alpha_q$ and PI3K was calculated to be 77 ± 25 nM. $G\alpha_q$·GTP[S] did not bind to the p110γ PI3K under these conditions (K_d > 1800 nM; see Fig. 3-3), suggesting that $G\alpha_q$ might selectively interact with class IA and not class IB PI3K isoforms. These results demonstrated that $G\alpha_q$ binds directly to the p110α/p85α PI3K, and active $G\alpha_q$ binds with a higher affinity than inactive $G\alpha_q$ [87].

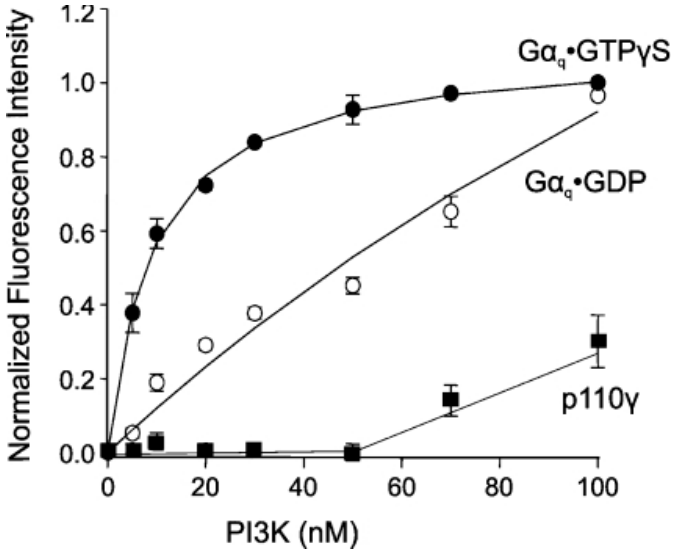

Fig. 3-3. Binding of $G\alpha_q$ to p110α /p85α PI3K using fluorescence spectroscopy. Purified recombinant p110α/p85α complex was titrated into a solution containing 5 nM coumarin-labeled $G\alpha_q$·GTP[S] (●) or $G\alpha_q$·GDP (○) reconstituted into 80 μM POPC/PS (2:1) LUVs. Recombinant p110γ was added to a solution containing 5 nM coumarin-labeled $G\alpha_q$·GTP[S] (■) in LUVs. The results shown are from three independent experiments performed in triplicate. GTPγS, GTP[S].

3-3-4. Ras binds to different PI3K isoforms *in vitro*

Ras is known to bind and activate p110α and p110β PI3K through the Ras-binding domain. To investigate if Ras binding to p110 is affected by different p85 subunits, I examined binding of purified K-Ras to purified p110α/p85α, p110α/p85β, p110β/p85α or p110β/p85β proteins. COS7 cells were transfected with the four FLAG epitope-tagged PI3K complexes. A FLAG antibody was used to immunoprecipitate the PI3Ks from cell lysates. Immunoprecipitates were washed and then incubated with a purified activated K-RasQ12V mutant *in vitro*. The mixture was then washed and analyzed by western blotting. The results show that the K-Ras protein coprecipitated with all combinations of PI3K p110/p85 subunits (Fig. 3-4). The blot was reprobed with the FLAG antibody to confirm the presence of p110 (Fig. 3-4). The expression of FLAG-p110 proteins was also confirmed by analyzing the cell lysates by western blotting using the FLAG antibody (Fig. 3-4).

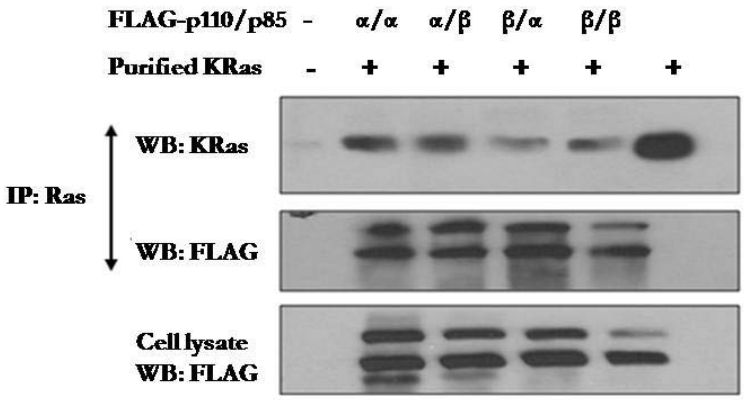

Fig. 3-4. Co-immunoprecipitation of Ras with different p110/p85 PI3K complexes. COS7 cells were transfected with FLAG-tagged PI3K complexes p110α/p85α, p110α/p85β, p110β/p85α, or p110β/p85β (α/α, α/β, β/α, or β/β, respectively). Cell lysates were immunoprecipitated (IP) with a FLAG antibody and the immunoprecipitates were mixed with purified activated K-RasQ12V (KRas) protein. Western blot (WB) analysis of the immunoprecipitates with a Ras antibody detected the presence of KRas (top panel). The blot was reprobed with the FLAG antibody to confirm the pull down of PI3K complexes (middle panel). Western blot analysis of cell lysate proteins confirmed the expression of PI3Ks (bottom panel).

3-3-5. $G\alpha_q$ interferes with H-Ras binding to p85α/p110α

We wondered if $G\alpha_q$ might also interfere with binding of PI3K to Ras as an additional mechanism to inhibit PI3K activation. I used fluorescence spectroscopy to first measure the K_d of p110α/p85α complex binding to H-Ras. Fluorescence intensity measurements were made after adding increasing amounts of PI3K to lipid vesicles preincubated with coumarin-labeled H-Ras. As expected, PI3K bound to active Ras·GTP[S] with a K_d of 31 ± 12 nM, while the K_d with inactive Ras·GDP was estimated to be at least 30 times higher (Fig. 3-5). When the lipid vesicles were reconstituted with coumarin-labeled Ras·GTP[S] in the presence of $G\alpha_q$·GTP[S], the specific binding between Ras and PI3K was greatly reduced (Fig. 3-5). This result indicates that activated $G\alpha_q$ interferes with H-Ras binding to p110α/p85α [87].

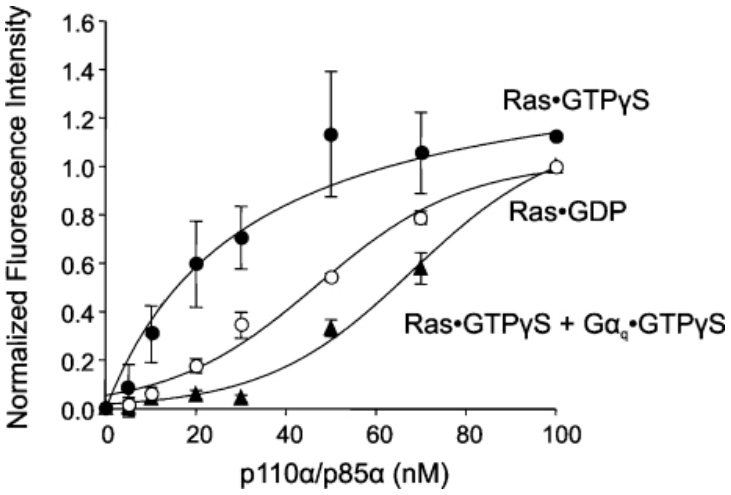

Fig. 3-5. Gα_q competes with Ras for binding to PI3K. LUVs were reconstituted with 10 nM coumarin-labeled Ras·GDP (○) or coumarin–Ras·GTP[S] without (●) or with (▲) 10 nM Gα_q·GTP[S]. Purified recombinant p110α/p85α was titrated into the solutions and fluorescence measurements were made. The results shown are from three independent experiments performed in triplicate. GTPγS, GTP[S].

3-3-6. Gα_q interferes with H-Ras activation of PI3K signaling

In addition to PI3K, Ras has a number of other direct targets, including the protein kinase Raf. We hypothesized that Gα_q should specifically inhibit the Ras/PI3K pathway and not the Ras/Raf pathway if Gα_q competes with Ras for binding to PI3K. To measure the effect of Gα_q on Ras/PI3K signaling, we assayed Akt activity in HEK-293 cells transfected with Akt–HA in the presence or absence of V12Ras and Gα_qQ209L. The protein kinase Akt is activated by the lipids produced by PI3K and its activity serves as an indirect measure of PI3K activity. Fig. 3-6A shows that Akt activity was almost three times higher in cells expressing V12Ras than in vector-transfected control cells, and this

increase was completely blocked by $G\alpha_qQ209L$. Western blotting showed that the amount of Akt–HA in each sample was similar (Fig. 3-6A inset).

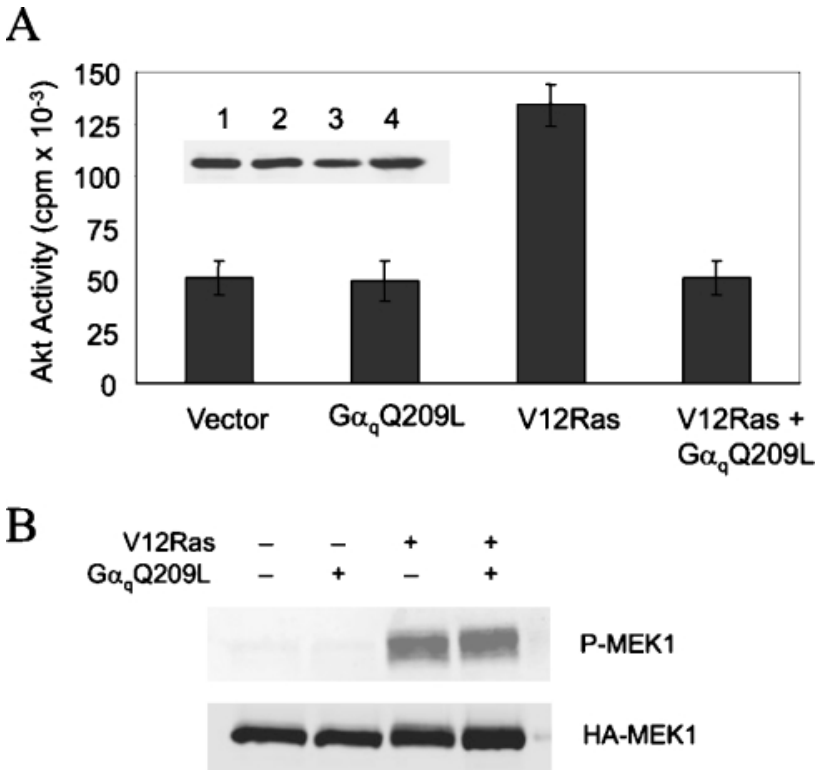

Fig. 3-6. Specific inhibition of the Ras/PI3K/Akt pathway by $G\alpha_q$. HEK-293 cells were co-transfected with (A) Akt–HA or (B) HA–MEK1 with or without V12Ras in the presence or absence of $G\alpha_qQ209L$. Cells were incubated in serum-free medium overnight prior to lysate preparation. (A) Akt activity was assayed in HA immunoprecipitates of cell lysates (mean±S.E.M.; *n*=3). The inset shows a western blot of cell lysates probed with HA antibody. (B) Activation of MEK1 was assessed on a western blot probed with phospho-MEK1/2 antibody (upper panel). The blot was reprobed with HA antibody (lower panel).

To assess the effect of $G\alpha_q$ on Ras/Raf signaling, we examined the phosphorylation of MEK1 at Ser217/Ser221. Binding of activated Ras to Raf leads to the phosphorylation and activation of MEK1. HEK-293 cells were transfected with HA–MEK1 in the presence or absence of V12Ras and $G\alpha_q$Q209L. Western blotting with a phospho-specific antibody showed that V12Ras activates MEK1, but $G\alpha_q$Q209L did not block this response (Fig. 3-6B). Reprobing the blot with HA antibody showed that the amount of HA–MEK1 was similar in each lane (Fig. 3-6B). These results indicate that active $G\alpha_q$ does not block all Ras effector pathways [87].

3-3-7. $G\alpha_q$ binds to the p85-binding domain of p110α

X-ray crystallography studies of the Ras·p110γ complex revealed that Ras binds to the Ras-binding domain (RBD) and the catalytic domain of p110γ [88]. Since $G\alpha_q$ blocks Ras binding to PI3K, we asked whether $G\alpha_q$ also binds to the RBD of p110α. We constructed GST fusion proteins encompassing the various domains of p110α and purified them from bacteria (Fig. 3-7A). These proteins were mixed with lysates of mammalian cells expressing HA-tagged $G\alpha_q$Q209L. The GST fusion proteins were pulled down with glutathione–Sepharose, and the presence of HA–$G\alpha_q$Q209L was assessed by western blotting. Surprisingly, we found that the p85-binding domain of p110α co-precipitated with HA–$G\alpha_q$Q209L, but the RBD did not (Fig. 3-7A). We also tested whether a FLAG-tagged p110α fragment (amino acids 118–1068) that does not contain the p85-binding domain co-immunoprecipitates with HA–$G\alpha_q$Q209L from extracts of COS7 cells expressing both proteins. FLAG–p110α amino acids 118–1068

exhibits substantial lipid kinase activity in an *in vitro* assay, indicating that the protein is folded correctly (results not shown). Consistent with our findings above using GST fusion proteins, FLAG–p110α amino acids 1–116 co-precipitated with HA–$G\alpha_q$Q209L, but FLAG–p110α amino acids 118–1068 did not (Fig. 3-7B). FLAG-tagged p110γ, which contains an RBD but lacks a p85-binding domain, also did not co-immunoprecipitate with co-transfected HA–$G\alpha_q$Q209L (Fig. 3-7B). Our laboratory showed earlier that the amount of p85α bound to p110α does not change in the presence of HA-$G\alpha_q$Q209L [37]. Therefore, even though activated $G\alpha_q$ binds to the p85α binding site on p110α, it does not inhibit PI3K activity by preventing formation of the p110α/p85α complex.

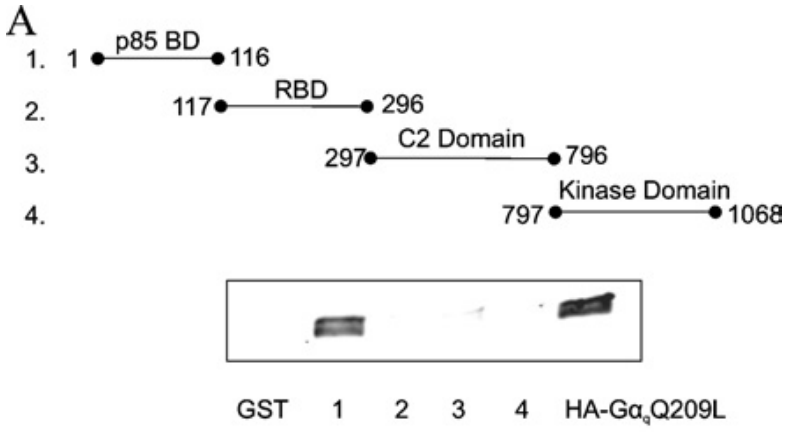

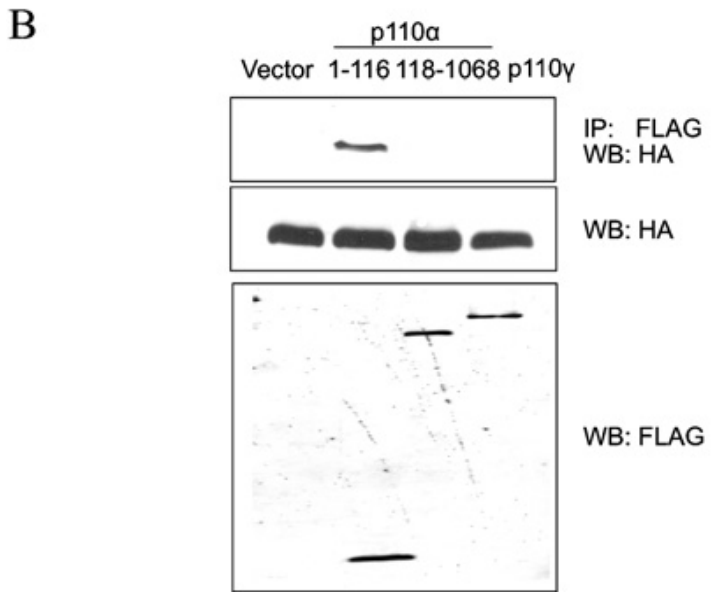

Fig. 3-7. $G\alpha_q$ binds to the p85-binding domain (p85 BD) of p110α. (A) Purified GST–p110α fusion proteins encompassing individual domains of p110α (50 ng) were immobilized on glutathione–Sepharose beads and mixed at 4 °C for 1 h with 250 μg of lysate proteins from FreeStyle 293 cells expressing HA–$G\alpha_q$Q209L. Cells were lysed in a buffer containing 1% Nonidet P40 plus 0.25% sodium deoxycholate (see the Materials and Methods section). The beads were washed with lysis buffer and bound proteins were analysed on a western blot probed with HA antibody. Native GST protein immobilized on beads was used as a negative control (first lane). The last lane is a sample of cell lysate expressing HA–$G\alpha_q$Q209L. The experiment was repeated with similar results. (B) COS7 cells were co-transfected with HA–$G\alpha_q$Q209L and either empty vector, FLAG–p110α amino acids 1–116, FLAG–p110α amino acids 118–1068 or FLAG–p110γ. Cell lysates were incubated with FLAG antibody and the immunoprecipitates were analysed on a western blot probed with HA antibody (top panel). Western blot analysis of total cell lysate proteins showed appropriate expression of HA–$G\alpha_q$Q209L and the various FLAG-tagged p110 proteins (bottom two panels). IP, immunoprecipitate; WB, western blot. The experiment was repeated with similar results.

3-3-8. $G\alpha_q$ binds to the p110-binding domain of p85α

In addition to binding of $G\alpha_q$ to the p85-binding domain of p110α, we wondered if $G\alpha_q$ can interact with the p85 subunit. I used fluorescence spectroscopy to first measure the K_d of p85α binding to $G\alpha_q$. Purified $G\alpha_q$ was activated with GTP[S], labeled with coumarin and reconstituted into lipid vesicles. Increasing concentrations of p85α were then titrated into the solution. Surprisingly, p85α bound to active $G\alpha_q$·GTP[S] with a K_d of 26 ± 3 nM (Fig. 3-8A), while the K_d with inactive $G\alpha_q$.GDP was higher (data not shown). This result indicates that activated $G\alpha_q$ binds to p85α independently of p110α.

Next, to determine the region where $G\alpha_q$ binds to p85α, I constructed FLAG-tagged truncation mutants of p85α (Fig. 3-8B). These p85α mutants were expressed in COS7 cells along with HA-$G\alpha_q$Q209L. Using immunoprecipitation with the FLAG antibody followed by western blotting, I confirmed that full-length p85α can pull down $G\alpha_q$Q209L (Fig. 3-8C). Furthermore, the p85α fragment containing amino acids 1-520 (mut.2) also co-precipitated with HA-$G\alpha_q$Q209L (Fig. 3-8B), suggesting that the C terminus of p85α is not required for binding. However, shorter p85α fragments (nSH2 and mut.1) were unable to pull down HA-$G\alpha_q$Q209L (Fig. 3-8A and B). These results suggest that $G\alpha_q$ binds to the p85α subunit in the helical coiled-coil domain (iSH2) between amino acids 514 and 520.

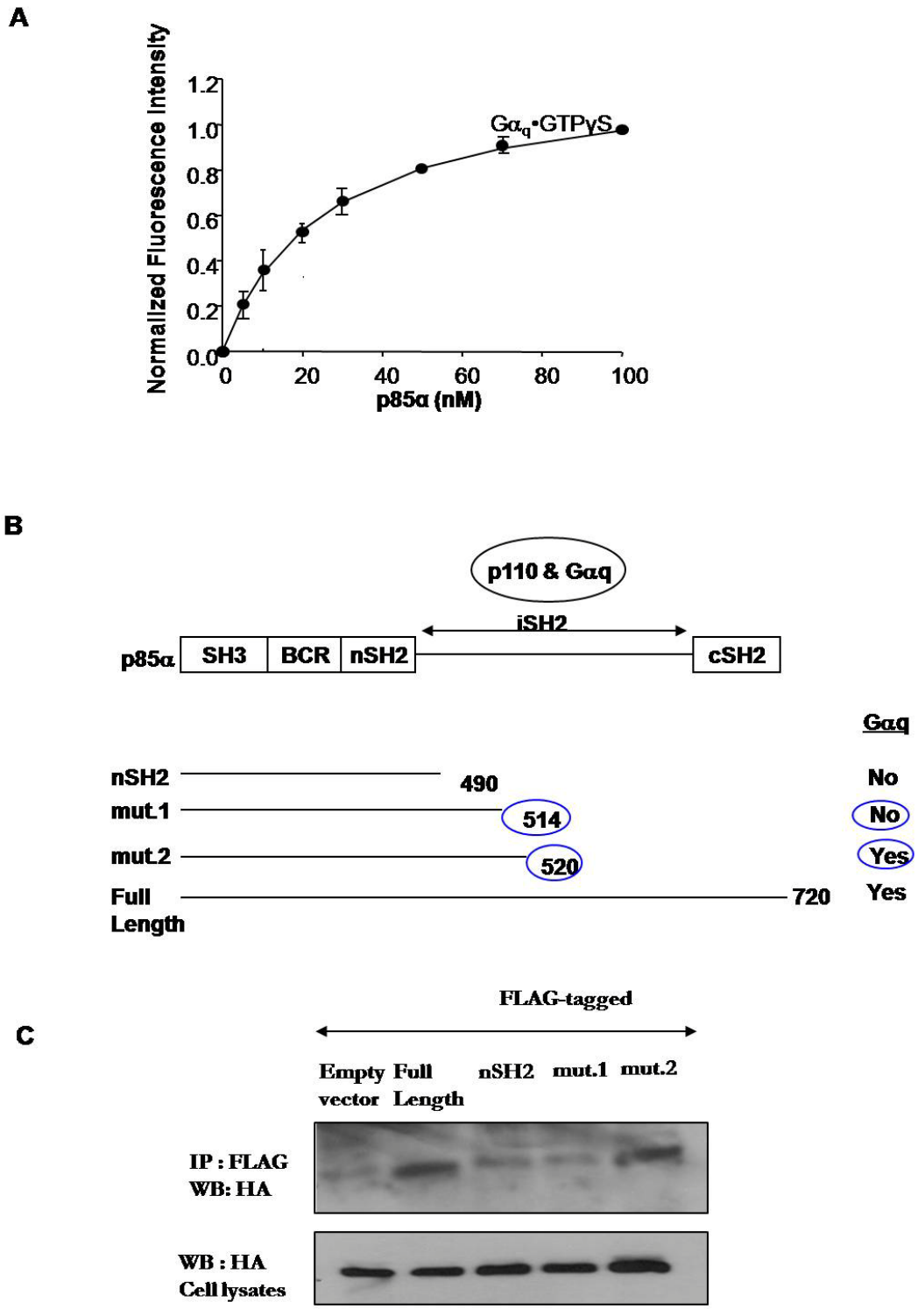

Fig. 3-8. Gα_q binds to the p110-binding domain (iSH2) of p85α. (A) Purified recombinant p85α protein was titrated into a solution containing 5 nM coumarin-labeled Gα_q·GTP[S]

reconstituted into 80 μM POPC/PS (2:1) LUVs. The results shown are from three independent experiments performed in triplicate. (B) Fragments of p85α were subcloned into p3XFLAG-CMV10 to make FLAG-nSH2 (1-490), FLAG-mut. 1 (1-514) and FLAG-mut. 2 (1-520). (C) COS7 cells were co-transfected with HA–$G\alpha_q$Q209L and either empty vector, FLAG–full length p85α, FLAG-nSH2, FLAG-mut. 1 or FLAG-mut. 2. Cell lysates were immunoprecipitated with FLAG antibody and the immunoprecipitates were analysed on a western blot probed with HA antibody (top panel). Western blot analysis of total cell lysate proteins showed appropriate expression of various HA–$G\alpha_q$Q209L -proteins (bottom panel). IP, immunoprecipitate; WB, western blot.

3-4. DISCUSSION

In this chapter, I demonstrated that activated $G\alpha_q$ can directly bind to PI3K complexes and that the binding causes a decrease in the lipid kinase activity of PI3Ks. We determined that $G\alpha_q$ binds to the p85-binding domain of p110α and does not appear to directly interact with the catalytic domain. Further, I showed that $G\alpha_q$ can bind to p85 alone in the iSH2 region independently of p110 binding. It remains unclear how these interactions lead to inhibition of lipid kinase activity. Binding of $G\alpha_q$ to p85α and p110α might induce a conformational change in the catalytic site that decreases the catalytic activity or the affinity for substrates. It will be of interest to determine if $G\alpha_q$ also binds to the p85-binding domain in p110δ. Since the amino acids in the region where $G\alpha_q$ binds to p85α are identical in p85β, I speculate that p85β will also interact with $G\alpha_q$ through this region. Future studies on point mutants in this region will provide further information about the interaction of p85 with $G\alpha_q$. Furthermore, additional studies to elucidate how $G\alpha_q$ inhibits PI3K will require the production of p110α mutants that cannot bind $G\alpha_q$ but that can still form a complex with p85.

The mechanism by which Ras activates PI3K is controversial. Conflicting studies point to either the RBD in p110α or the iSH2 domain in p85α as playing a dominant role in mediating the activating effect of Ras on PI3K [22, 89]. The crystal structure of a Ras·p110γ complex shows that Ras makes direct contacts with both the RBD and the C-terminal lobe of the PI3K catalytic domain [88]. Ras binding to p110γ induces conformational changes that affect the putative phosphatidylinositol headgroup binding site and may result in a change of affinity for substrate [88]. Regardless of the exact

mechanism for Ras activation, we found that $G\alpha_q$ blocks Ras from binding to PI3K and completely suppresses Ras activation of PI3K signaling. $G\alpha_q$ does not appear to compete directly for Ras binding to p110α, since it does not bind to the RBD. Instead, $G\alpha_q$ binding to PI3K may induce a structural change that disrupts its ability to bind Ras. The fact that $G\alpha_q$Q209L completely blocked Ras activation of PI3K might be due to suppression of intrinsic PI3K activity combined with the additional effect of $G\alpha_q$ in blocking Ras from binding to PI3K. This result provides a mechanism to explain how $G\alpha_q$ attenuates PI3K signaling in the absence of PLCβ activation.

Activation of G_q-coupled receptors can have complex effects on PI3K signaling. These receptors can activate more than one type of Gα subunit, and the dissociated Gβγ dimers can signal independently to affect specific proteins. Although activated $G\alpha_q$ inhibits p110α, p110γ is activated in response to the stimulation of these receptors and p110β is thought to be activated by GPCRs. Direct binding of Gβγ to p110γ and p110β was found to activate these enzymes [32, 90]. In cell types that express multiple PI3K catalytic and regulatory subunits, different p110/p85 complexes may be differentially regulated by $G\alpha_q$. Therefore, attributing an effect on PI3K to a particular G protein subunit after receptor activation can be difficult. Our studies that examine the interactions between $G\alpha_q$ and PI3K complexes may lead to a better understanding of the crosstalk between pathways that use these signaling molecules.

Chapter 4.

General Discussion and Future Work

The data presented in this dissertation show that class IA PI3K isoforms have distinct biological roles in the liver and that these enzymes are regulated by heterotrimeric G proteins. In chapter 2, I provided evidence that ablation of p110α, but not p110β, blocks HFD- induced liver steatosis. Reduced fatty acid uptake due to decreased mRNA and protein levels of L-FABP is most likely the cause for the decreased triglyceride accumulation. I also showed that p110β affects glucose homeostasis in mice fed regular chow by suppressing cAMP levels in hepatocytes. These results suggest that p110α and p110β have distinct roles in regulating hepatic lipid and glucose metabolism and reveal previously unknown functions of class IA PI3K catalytic subunits. In chapter 3, I demonstrated that $G\alpha_q$ directly binds to PI3Ks and inhibits their catalytic activity. These results suggest that PI3Ks are novel signaling effectors of $G\alpha_q$.

PI3K signaling plays a central role in insulin regulation of glucose metabolism. Knockout and transgenic mouse models have provided *in vivo* evidence to support the role of dysfunctional PI3K recruitment/activation in the development of diabetes. For example, targeted disruption of IRS-2 impaired PI3K activation and resulted in an overt diabetic phenotype [91]. Impaired insulin-stimulated PI3K activation has also been observed in skeletal muscle and adipose tissue of patients with type 2 diabetes [92]. In adipocytes and myocytes, insulin-mediated glucose uptake and membrane translocation of the glucose transporter GLUT4 were blocked by dominant negative forms of Akt or by RNAi against Akt2 [93]. In hepatocytes, it was demonstrated that PI3K/Akt signaling inhibits FoxO1-mediated transcription of gluconeogenic genes and therefore suppresses glucose production [94].

Although the PI3K pathway is clearly involved in the regulation of glucose metabolism, the isoform-specific functions of PI3K in this process remain unclear. The relative contribution of individual PI3K regulatory and catalytic isoforms is now starting to be addressed using genetically modified mice. Homozygous pan-p85α knockout (p85α + p55α + p50α) mice were perinatally lethal [95]. Individual p85α and p85β knockout mice were viable but hypoglycemic [96-97]. Whole body p110α or p110β knockout mice died as embryos [98-99]. Whole body p110δ mice were viable with impaired immune functions but no metabolic phenotype [100]. Replacement of one copy of the p110α gene with a kinase-dead p110α mutant in the whole body resulted in glucose intolerance [101]. Whole body replacement of both copies of p110β with a kinase-dead p110β mutant resulted in mild insulin resistance with age [102].

It is believed that defective PI3K signaling in many tissues contributes collectively to the complex metabolic defects associated with type 2 diabetes. Since the liver is one of the most important hormone-responsive organs that regulate glucose homeostasis, I investigated the roles of the p110α and p110β isoforms in the mouse liver. As expected based on the literature, insulin signaling to the PI3K/Akt pathway was attenuated in the $p110\alpha^{-/-}$ liver. Somewhat surprisingly, this signaling defect did not lead to hyperglycemia and hyperinsulinemia in the whole animal. However, I did find that the glycogen level was greatly reduced in the $p110\alpha^{-/-}$ liver. This is probably related to reduced Akt activation that resulted in upregulation of G6PC levels. As expected, I found that insulin signaling to the PI3K/Akt pathway in the liver was unaffected by loss of p110β. On the other hand, I was surprised to find that $p110\beta^{-/-}$ hepatocytes exhibited an increased rate of glycogenolysis and gluconeogensis that was associated with

hyperglycemia and hyperinsulinemia in the whole animal. I believe this is due to an increased level of cAMP in these knockout hepatocytes, which is probably responsible for the increased PEPCK and G6PC gene expression observed in the $p110\beta^{-/-}$ liver.

Despite their similar structure and substrate specificity, I showed in chapter 3 that the specific activity of p110α and p110β are very different. Thus, the differences in function could be due to differences in their catalytic activity. Alternatively, the two PI3K isoforms might phosphorylate different pools of PIP_2 in different intracellular compartments, which might account for their isoform-specific functions. Future studies in cells transfected with fluorescent-tagged constitutively active p110α or p110β mutants and immunohistochemical analysis with antibodies specific to each isoform or downstream effectors will help to determine the subcellular localization of these enzymes.

It has been reported that p110β regulates some processes, such as cell proliferation, trafficking [60, 102] and autophagy (data not published yet), independently of its catalytic activity. Because the PI3K proteins are deleted in our mouse models, this raises the possibility that regulation of metabolism by PI3K isoforms could also be independent of their kinase activity. Reconstitution experiments using adenovirus to express kinase-dead p110α or p110β mutants in the appropriate knockout hepatocytes could address this question. Treating the control hepatocytes with isoform-specific PI3K inhibitors is another approach. For example, $p110\beta^{+/+}$ hepatocytes could be treated with TGX-221 (a p110β-specific inhibitor) to determine if decreased p110β catalytic activity results in increased rates of gluconeogenesis and glycogenolysis. Similarly, $p110\alpha^{+/+}$ hepatocytes could be treated with a p110α-specific inhibitor to determine if p110α

catalytic activity controls fatty acid uptake and L-FABP expression. Like our knockout mice, whole body kinase-dead p110β mice exhibited decreased hepatic glycogen levels, suggesting that this phenotype, at least, is due to loss of catalytic function [102]. It would be interesting to determine if hepatocytes from these mice have increased cAMP and Adcy-5 levels.

Akt and PKCζ are both downstream effectors of PI3K. My data in the HFD feeding study suggest that PKCζ rather than Akt is involved in the lipid phenotype of $p110\alpha^{-/-}$ mice. Adenoviral delivery of constitutively active forms of Akt or PKCζ into $p110\alpha^{-/-}$ hepatocytes followed by fatty uptake assays could clarify whether Akt or PKCζ plays a role in this lipid phenotype. Conversely, control cells could be treated with either Akt or PKCζ inhibitors to determine if fatty acid uptake is reduced. Similar studies could be done to determine if PKCζ regulates the expression of L-FABP.

My data strongly suggest that ablation of p110β in the liver resulted in higher cAMP and adenylyl cyclase levels to alter glucose metabolism. Future studies by western blotting will determine if the Adcy-5 protein level is decreased. Additional studies can be pursued to identify transcription factors downstream of p110β that regulate the expression of Adcy-5. Translocation of active p110β to the nucleus might be part of the mechanism of gene regulation. Interestingly, recent studies have shown increased nuclear localization of p110β in response to IGF-1 and platelet-derived growth factor (PDGF) activation in some cell lines [103]. Since p110β is also activated by GPCRs, further studies are needed to investigate if activation of these receptors induces translocation of p110β to the nucleus to regulate expression of Adcy-5.

As discussed in chapter 3, class IA PI3Ks are regulated by the heterotrimeric G protein $G\alpha_q$. I provided evidence that $G\alpha_q$ directly binds to and inhibits the PI3K complexes p110α/p85α, p110α/p85β, p110β/p85α and p110β/p85β. In addition, the binding of $G\alpha_q$ to PI3K blocked Ras binding to PI3K and selectively inhibited Ras activation of the PI3K signaling pathway. Interestingly, $G\alpha_q$ did not bind to the Ras-binding domain on p110α, but instead to the p85-binding domain. Furthermore, $G\alpha_q$ can also bind directly to the p85α subunit. Additional structural studies could reveal the details of how $G\alpha_q$ block Ras binding to p110α. This information could be useful for the development of strategies to specifically block Ras activation of PI3K.

Ras is an oncogene that is activated by mutation in approximately 25% of all human tumors. The oncogenic capability of Ras is at least partly transmitted through its signaling to class I PI3K family members [104], [60]. Previous studies showed that Ras-dependent PI3K activation was essential for anchorage-independent growth and cytoskeletal reorganization associated with transformation [22]. Recently the importance of the interaction of p110α with Ras in tumorigenesis was demonstrated *in vivo* by expressing in mice a p110α point mutant that cannot bind Ras [104]. These mice were completely resistant to oncogenic K-Ras-induced lung tumorigenesis.

Ras proteins are potential drug targets for the treatment of cancer. One approach to inhibiting oncogenic Ras proteins would be to design compounds that strengthen their GTPase activity. However, the design of such gain-of-function compounds is difficult and none exist so far. Currently the only available inhibitors of Ras in clinical trials are farnesyl transferase inhibitors that block lipid modification and membrane targeting of Ras. So far these drugs have met with minimal clinical success because there are many

Ras-like proteins that are also affected by these drugs. Since the Ras-PI3K interaction is critical for tumor formation, another strategy to inhibit oncogenic Ras would be to block its interaction with PI3K. In chapter 3, I showed that stimulated $G\alpha_q$ interfered with Ras binding and activation of the p110α/p85α complex. Further structural studies could determine the nature of the interaction between these proteins. Understanding this interaction may aid in the development of small molecule inhibitors or peptide drugs to block binding of Ras to PI3K. Selective inhibition of a specific Ras-activated signaling pathway could cause less toxicity than a PI3K inhibitor because it would not inhibit basal PI3K activity. However, the selectivity of such a drug against different PI3K complexes might be weak, since I showed in chapter 3 that Ras and $G\alpha_q$ bound to four different p110α and p110β complexes.

Direct inhibition of PI3K by $G\alpha_q$ is probably not the only mechanism by which G_q-coupled receptors inhibit PI3K signaling. Our laboratory reported that stimulation of the α_{1A} adrenergic receptor in Rat-1 cells inhibited PDGF-induced binding of PI3K to the PDGF receptor [105]. This response was due to enhanced dephosphorylation of the PDGF receptor at Tyr751, which forms a docking site for PI3K, by SHP-2 (an SH2 domain-containing protein tyrosine phosphatase). Activation of M3 muscarinic receptors in 1321N1 astrocytoma cells similarly blocked insulin-induced IRS-1 tyrosine phosphorylation and recruitment of PI3K. However, this was apparently a consequence of increased serine phosphorylation of IRS-1, which uncouples it from insulin-induced tyrosine phosphorylation [106]. Finally, activation of $G\alpha_q$ in cardiac myocytes was proposed to decrease PI3K signaling due to depletion of intracellular PIP_2, which is a substrate for both PLCβ and PI3K [107]. One difference between the latter two

mechanisms cited above and the one reported in chapter 3 is their dependence on PLCβ activation.

The inhibitory effect of $G\alpha_q$ on PI3K signaling could have physiological consequences for hepatic glucose and lipid metabolism. It was shown years ago that G_q-coupled receptors inhibit glycogen synthase and counteract the effect of insulin in hepatocytes [108-109]. It is now known that PI3K plays a key role in regulating glycogen metabolism, and I believe that $G\alpha_q$ inhibition of PI3K may partly explain why activation of these receptors antagonizes insulin responses. I could address this research question using a strategy developed by our laboratory in which a fusion protein of $G\alpha_q$Q209L with the hormone-binding domain of the estrogen receptor (hbER) is activated by exogenous tamoxifen. Our laboratory generated transgenic mice expressing this fusion protein to demonstrate that inhibition of PI3K by $G\alpha_q$ in the heart reduces L-type Ca^{2+} channel function [110]. Potentially, transgenic mice expressing the $G\alpha_q$Q209L-hbER protein in the liver under the control of an albumin promoter could be generated. These tamoxifen-activated $G\alpha_q$ transgenic mice would allow me to investigate the consequence of $G\alpha_q$ inhibition of PI3K in the liver. For example, I could determine if these animals develop glucose intolerance after tamoxifen injection. This could be due to inhibition of p110β by $G\alpha_q$, leading to increased cAMP and Adcy-5 levels. Activation of $G\alpha_q$ might also block HFD- induced liver steatosis. This could be due to inhibition of p110α by $G\alpha_q$ and thus a reduction in fatty acid uptake in hepatocytes.

GENERAL CONCLUSION

The PI3K signaling pathway is critical in the signal transduction circuitry that regulates essential cellular functions. Dysregulated PI3K signaling occurs frequently in human diseases. Therefore, PI3Ks have become promising targets for therapeutic interventions. Indeed, a few PI3K inhibitors are already in phase 1/2 clinical trials for the treatment of cancer. However, these inhibitors are not isoform specific. My research revealed that in the liver, p110α and p110β PI3Ks have distinct metabolic roles. Furthermore, complex regulation of the PI3K isoforms by G proteins might contribute to diversity in their function and signaling which might be non-redundant. Hence, my research suggests that pan-PI3K inhibitors might have metabolic side effects and caution must be taken in treating cancer patients who are obese, diabetic or at a high risk for developing glucose intolerance.

The continuing development of tissue-specific transgenic and knockout mice as well as isoform-specific pharmacological inhibitors will help to determine functional specificity of PI3K isoforms in the future. Biochemical and structural exploration is also likely to provide important insights into their mode of regulation. Nevertheless, since its discovery more than 20 years ago, tremendous progress has been made in our understanding of the diverse biological roles and regulation of PI3K isoforms. This puts us in a much better position to manipulate the pathway therapeutically. Therefore, with well-grounded optimism, I anticipate that in the near future therapeutic agents targeting the PI3K pathway will show their promise in patients with diseases such as cancer and diabetes.

REFERENCES

1. Whitman, M., et al., *Association of phosphatidylinositol kinase activity with polyoma middle-T competent for transformation.* Nature, 1985. **315**(6016): p. 239-42.

2. Whitman, M., et al., *Type I phosphatidylinositol kinase makes a novel inositol phospholipid, phosphatidylinositol-3-phosphate.* Nature, 1988. **332**(6165): p. 644-6.

3. Ling, L.E., et al., *Transformation-defective mutants of polyomavirus middle T antigen associate with phosphatidylinositol 3-kinase (PI 3-kinase) but are unable to maintain wild-type levels of PI 3-kinase products in intact cells.* J Virol, 1992. **66**(3): p. 1702-8.

4. Serunian, L.A., et al., *Production of novel polyphosphoinositides in vivo is linked to cell transformation by polyomavirus middle T antigen.* J Virol, 1990. **64**(10): p. 4718-25.

5. Hiles, I.D., et al., *Phosphatidylinositol 3-kinase: structure and expression of the 110 kd catalytic subunit.* Cell, 1992. **70**(3): p. 419-29.

6. Vanhaesebroeck, B., et al., *Phosphoinositide 3-kinases: a conserved family of signal transducers.* Trends Biochem Sci, 1997. **22**(7): p. 267-72.

7. Vanhaesebroeck, B., et al., *P110delta, a novel phosphoinositide 3-kinase in leukocytes.* Proc Natl Acad Sci U S A, 1997. **94**(9): p. 4330-5.

8. Cannizzaro, L.A., et al., *The human gene encoding phosphatidylinositol-3 kinase associated p85 alpha is at chromosome region 5q12-13.* Cancer Res, 1991. **51**(14): p. 3818-20.

9. Carpenter, C.L. and L.C. Cantley, *Phosphoinositide kinases.* Biochemistry, 1990. **29**(51): p. 11147-56.

10. Carpenter, C.L., et al., *Purification and characterization of phosphoinositide 3-kinase from rat liver.* J Biol Chem, 1990. **265**(32): p. 19704-11.

11. Escobedo, J.A., et al., *cDNA cloning of a novel 85 kd protein that has SH2 domains and regulates binding of PI3-kinase to the PDGF beta-receptor.* Cell, 1991. **65**(1): p. 75-82.

12. Skolnik, E.Y., et al., *Cloning of PI3 kinase-associated p85 utilizing a novel method for expression/cloning of target proteins for receptor tyrosine kinases.* Cell, 1991. **65**(1): p. 83-90.

13. Fruman, D.A., L.C. Cantley, and C.L. Carpenter, *Structural organization and alternative splicing of the murine phosphoinositide 3-kinase p85 alpha gene.* Genomics, 1996. **37**(1): p. 113-21.

14. Inukai, K., et al., *p85alpha gene generates three isoforms of regulatory subunit for phosphatidylinositol 3-kinase (PI 3-Kinase), p50alpha, p55alpha, and p85alpha, with different PI 3-kinase activity elevating responses to insulin.* J Biol Chem, 1997. **272**(12): p. 7873-82.

15. Pons, S., et al., *The structure and function of p55PIK reveal a new regulatory subunit for phosphatidylinositol 3-kinase.* Mol Cell Biol, 1995. **15**(8): p. 4453-65.

16. Pirola, L., et al., *Activation loop sequences confer substrate specificity to phosphoinositide 3-kinase alpha (PI3Kalpha). Functions of lipid kinase-deficient PI3Kalpha in signaling.* J Biol Chem, 2001. **276**(24): p. 21544-54.

17. Hu, P., et al., *Cloning of a novel, ubiquitously expressed human phosphatidylinositol 3-kinase and identification of its binding site on p85.* Mol Cell Biol, 1993. **13**(12): p. 7677-88.

18. Musacchio, A., L.C. Cantley, and S.C. Harrison, *Crystal structure of the breakpoint cluster region-homology domain from phosphoinositide 3-kinase p85 alpha subunit.* Proc Natl Acad Sci U S A, 1996. **93**(25): p. 14373-8.

19. Weinkove, D., et al., *p60 is an adaptor for the Drosophila phosphoinositide 3-kinase, Dp110.* J Biol Chem, 1997. **272**(23): p. 14606-10.

20. Yu, J., C. Wjasow, and J.M. Backer, *Regulation of the p85/p110alpha phosphatidylinositol 3'-kinase. Distinct roles for the n-terminal and c-terminal SH2 domains.* J Biol Chem, 1998. **273**(46): p. 30199-203.

21. Rodriguez-Viciana, P., et al., *Phosphatidylinositol-3-OH kinase as a direct target of Ras.* Nature, 1994. **370**(6490): p. 527-32.

22. Rodriguez-Viciana, P., et al., *Activation of phosphoinositide 3-kinase by interaction with Ras and by point mutation.* EMBO J, 1996. **15**(10): p. 2442-51.

23. Cuevas, B.D., et al., *Tyrosine phosphorylation of p85 relieves its inhibitory activity on phosphatidylinositol 3-kinase.* J Biol Chem, 2001. **276**(29): p. 27455-61.

24. Song, G., G. Ouyang, and S. Bao, *The activation of Akt/PKB signaling pathway and cell survival.* J Cell Mol Med, 2005. **9**(1): p. 59-71.

25. Dhanasekaran, N., et al., *Regulation of cell proliferation by G proteins.* Oncogene, 1998. **17**(11 Reviews): p. 1383-94.

26. Simon, M.I., M.P. Strathmann, and N. Gautam, *Diversity of G proteins in signal transduction.* Science, 1991. **252**(5007): p. 802-8.

27. Jiang, Y., et al., *The G protein G alpha12 stimulates Bruton's tyrosine kinase and a rasGAP through a conserved PH/BM domain.* Nature, 1998. **395**(6704): p. 808-13.

28. Meigs, T.E., et al., *Interaction of Galpha 12 and Galpha 13 with the cytoplasmic domain of cadherin provides a mechanism for beta -catenin release.* Proc Natl Acad Sci U S A, 2001. **98**(2): p. 519-24.

29. Zhu, D., et al., *Galpha12 directly interacts with PP2A: evidence FOR Galpha12-stimulated PP2A phosphatase activity and dephosphorylation of microtubule-associated protein, tau.* J Biol Chem, 2004. **279**(53): p. 54983-6.

30. Guillermet-Guibert, J., et al., *The p110beta isoform of phosphoinositide 3-kinase signals downstream of G protein-coupled receptors and is functionally redundant with p110gamma.* Proc Natl Acad Sci U S A, 2008. **105**(24): p. 8292-7.

31. Kubo, H., et al., *Specific role for p85/p110beta in GTP-binding-protein-mediated activation of Akt.* Biochem J, 2005. **392**(Pt 3): p. 607-14.

32. Kurosu, H., et al., *Heterodimeric phosphoinositide 3-kinase consisting of p85 and p110beta is synergistically activated by the betagamma subunits of G proteins and phosphotyrosyl peptide.* J Biol Chem, 1997. **272**(39): p. 24252-6.

33. Maier, U., A. Babich, and B. Nurnberg, *Roles of non-catalytic subunits in gbetagamma-induced activation of class I phosphoinositide 3-kinase isoforms beta and gamma.* J Biol Chem, 1999. **274**(41): p. 29311-7.

34. Katada, T., et al., *Synergistic activation of a family of phosphoinositide 3-kinase via G-protein coupled and tyrosine kinase-related receptors.* Chem Phys Lipids, 1999. **98**(1-2): p. 79-86.

35. Tang, X., et al., *Role of phosphatidylinositol 3-kinase and specific protein kinase B isoforms in the suppression of apoptosis mediated by the Abelson protein-tyrosine kinase.* J Biol Chem, 2000. **275**(17): p. 13142-8.

36. Imamura, T., et al., *Endothelin-1-induced GLUT4 translocation is mediated via Galpha(q/11) protein and phosphatidylinositol 3-kinase in 3T3-L1 adipocytes.* J Biol Chem, 1999. **274**(47): p. 33691-5.

37. Ballou, L.M., et al., *Activated G alpha q inhibits p110 alpha phosphatidylinositol 3-kinase and Akt.* J Biol Chem, 2003. **278**(26): p. 23472-9.

38. Althoefer, H., P. Eversole-Cire, and M.I. Simon, *Constitutively active Galphaq and Galpha13 trigger apoptosis through different pathways.* J Biol Chem, 1997. **272**(39): p. 24380-6.

39. Ueda, H., et al., *Galphaq/11 signaling induces apoptosis through two pathways involving reduction of Akt phosphorylation and activation of RhoA in HeLa cells.* Exp Cell Res, 2004. **298**(1): p. 207-17.

40. Sopasakis, V.R., et al., *Specific roles of the p110alpha isoform of phosphatidylinsositol 3-kinase in hepatic insulin signaling and metabolic regulation.* Cell Metab, 2010. **11**(3): p. 220-30.

41. Taniguchi, C.M., et al., *Divergent regulation of hepatic glucose and lipid metabolism by phosphoinositide 3-kinase via Akt and PKClambda/zeta.* Cell Metab, 2006. **3**(5): p. 343-53.

42. Standaert, M.L., et al., *Insulin activates protein kinases C-zeta and C-lambda by an autophosphorylation-dependent mechanism and stimulates their translocation to GLUT4 vesicles and other membrane fractions in rat adipocytes.* J Biol Chem, 1999. **274**(36): p. 25308-16.

43. Cross, D.A., et al., *Inhibition of glycogen synthase kinase-3 by insulin mediated by protein kinase B.* Nature, 1995. **378**(6559): p. 785-9.

44. Zhang, X., et al., *Phosphorylation of serine 256 suppresses transactivation by FKHR (FOXO1) by multiple mechanisms. Direct and indirect effects on nuclear/cytoplasmic shuttling and DNA binding.* J Biol Chem, 2002. **277**(47): p. 45276-84.

45. Farese, R.V., M.P. Sajan, and M.L. Standaert, *Atypical protein kinase C in insulin action and insulin resistance.* Biochem Soc Trans, 2005. **33**(Pt 2): p. 350-3.

46. Matsumoto, M., et al., *PKClambda in liver mediates insulin-induced SREBP-1c expression and determines both hepatic lipid content and overall insulin sensitivity.* J Clin Invest, 2003. **112**(6): p. 935-44.

47. Buettner, R., et al., *Defining high-fat-diet rat models: metabolic and molecular effects of different fat types.* J Mol Endocrinol, 2006. **36**(3): p. 485-501.

48. Inoue, M., et al., *Increased expression of PPARgamma in high fat diet-induced liver steatosis in mice.* Biochem Biophys Res Commun, 2005. **336**(1): p. 215-22.

49. Leavens, K.F., et al., *Akt2 is required for hepatic lipid accumulation in models of insulin resistance.* Cell Metab, 2009. **10**(5): p. 405-18.

50. Newberry, E.P., et al., *Diet-induced obesity and hepatic steatosis in L-Fabp / mice is abrogated with SF, but not PUFA, feeding and attenuated after cholesterol supplementation.* Am J Physiol Gastrointest Liver Physiol, 2008. **294**(1): p. G307-14.

51. Lu, Z., et al., *Loss of cardiac phosphoinositide 3-kinase p110 alpha results in contractile dysfunction.* Circulation, 2009. **120**(4): p. 318-25.

52. Ballou, L.M., et al., *Differential regulation of the phosphatidylinositol 3-kinase/Akt and p70 S6 kinase pathways by the alpha(1A)-adrenergic receptor in rat-1 fibroblasts.* J Biol Chem, 2000. **275**(7): p. 4803-9.

53. Ballou, L.M., et al., *Dual regulation of glycogen synthase kinase-3beta by the alpha1A-adrenergic receptor.* J Biol Chem, 2001. **276**(44): p. 40910-6.

54. Seglen, P.O., *Preparation of isolated rat liver cells.* Methods Cell Biol, 1976. **13**: p. 29-83.

55. Shih, M. and C.C. Malbon, *Oligodeoxynucleotides antisense to mRNA encoding protein kinase A, protein kinase C, and beta-adrenergic receptor kinase reveal distinctive cell-type-specific roles in agonist-induced desensitization.* Proc Natl Acad Sci U S A, 1994. **91**(25): p. 12193-7.

56. Fan, G., et al., *A transgenic mouse model of heart failure using inducible Galpha q.* J Biol Chem, 2005. **280**(48): p. 40337-46.

57. Berk, P.D., S. Zhou, and M.W. Bradbury, *Increased hepatocellular uptake of long chain fatty acids occurs by different mechanisms in fatty livers due to obesity or excess ethanol use, contributing to development of steatohepatitis in both settings.* Trans Am Clin Climatol Assoc, 2005. **116**: p. 335-44; discussion 345.

58. Bradbury, M.W., *Lipid metabolism and liver inflammation. I. Hepatic fatty acid uptake: possible role in steatosis.* Am J Physiol Gastrointest Liver Physiol, 2006. **290**(2): p. G194-8.

59. Bradbury, M.W. and P.D. Berk, *Lipid metabolism in hepatic steatosis.* Clin Liver Dis, 2004. **8**(3): p. 639-71, xi.

60. Jia, S., et al., *Essential roles of PI(3)K-p110beta in cell growth, metabolism and tumorigenesis.* Nature, 2008. **454**(7205): p. 776-9.

61. Sadana, R. and C.W. Dessauer, *Physiological roles for G protein-regulated adenylyl cyclase isoforms: insights from knockout and overexpression studies.* Neurosignals, 2009. **17**(1): p. 5-22.

62. Donnelly, K.L., et al., *Sources of fatty acids stored in liver and secreted via lipoproteins in patients with nonalcoholic fatty liver disease.* J Clin Invest, 2005. **115**(5): p. 1343-51.

63. Sajan, M.P., et al., *The critical role of atypical protein kinase C in activating hepatic SREBP-1c and NFkappaB in obesity.* J Lipid Res, 2009. **50**(6): p. 1133-45.

64. Mao, J., et al., *Liver-specific deletion of acetyl-CoA carboxylase 1 reduces hepatic triglyceride accumulation without affecting glucose homeostasis.* Proc Natl Acad Sci U S A, 2006. **103**(22): p. 8552-7.

65. Delgado, T.C., et al., *Sources of hepatic triglyceride accumulation during high-fat feeding in the healthy rat.* NMR Biomed, 2009. **22**(3): p. 310-7.

66. Oosterveer, M.H., et al., *High fat feeding induces hepatic fatty acid elongation in mice.* PLoS One, 2009. **4**(6): p. e6066.

67. Martin, G.G., et al., *Decreased liver fatty acid binding capacity and altered liver lipid distribution in mice lacking the liver fatty acid-binding protein gene.* J Biol Chem, 2003. **278**(24): p. 21429-38.

68. Luxon, B.A., M.T. Milliano, and R.A. Weisiger, *Induction of hepatic cytosolic fatty acid binding protein with clofibrate accelerates both membrane and cytoplasmic transport of palmitate.* Biochim Biophys Acta, 2000. **1487**(2-3): p. 309-18.

69. Murphy, E.J., *L-FABP and I-FABP expression increase NBD-stearate uptake and cytoplasmic diffusion in L cells.* Am J Physiol, 1998. **275**(2 Pt 1): p. G244-9.

70. Newberry, E.P., et al., *Decreased hepatic triglyceride accumulation and altered fatty acid uptake in mice with deletion of the liver fatty acid-binding protein gene.* J Biol Chem, 2003. **278**(51): p. 51664-72.

71. Newberry, E.P., et al., *Protection against Western diet-induced obesity and hepatic steatosis in liver fatty acid-binding protein knockout mice.* Hepatology, 2006. **44**(5): p. 1191-205.

72. Brandes, R., et al., *Induction of fatty acid binding protein by peroxisome proliferators in primary hepatocyte cultures and its relationship to the induction of peroxisomal beta-oxidation.* Biochim Biophys Acta, 1990. **1034**(1): p. 53-61.

73. Jacinto, E., et al., *SIN1/MIP1 maintains rictor-mTOR complex integrity and regulates Akt phosphorylation and substrate specificity.* Cell, 2006. **127**(1): p. 125-37.

74. Xu, C., et al., *Metabolic dysregulation in the SHROB rat reflects abnormal expression of transcription factors and enzymes that regulate carbohydrate metabolism.* J Nutr Biochem, 2008. **19**(5): p. 305-12.

75. Erraji-Benchekroun, L., et al., *Overexpression of beta2-adrenergic receptors in mouse liver alters the expression of gluconeogenic and glycolytic enzymes.* Am J Physiol Endocrinol Metab, 2005. **288**(4): p. E715-22.

76. Crackower, M.A., et al., *Regulation of myocardial contractility and cell size by distinct PI3K-PTEN signaling pathways.* Cell, 2002. **110**(6): p. 737-49.

77. Patrucco, E., et al., *PI3Kgamma modulates the cardiac response to chronic pressure overload by distinct kinase-dependent and -independent effects.* Cell, 2004. **118**(3): p. 375-87.

78. Okumura, S., et al., *Disruption of type 5 adenylyl cyclase gene preserves cardiac function against pressure overload.* Proc Natl Acad Sci U S A, 2003. **100**(17): p. 9986-90.

79. Okumura, S., et al., *Type 5 adenylyl cyclase disruption alters not only sympathetic but also parasympathetic and calcium-mediated cardiac regulation.* Circ Res, 2003. **93**(4): p. 364-71.

80. Iwamoto, T., et al., *Motor dysfunction in type 5 adenylyl cyclase-null mice.* J Biol Chem, 2003. **278**(19): p. 16936-40.

81. Homan, R. and K.L. Hamelehle, *Phospholipase A2 relieves phosphatidylcholine inhibition of micellar cholesterol absorption and transport by human intestinal cell line Caco-2.* J Lipid Res, 1998. **39**(6): p. 1197-209.

82. Zhang, S., et al., *A C-terminal mutant of the G protein beta subunit deficient in the activation of phospholipase C-beta.* J Biol Chem, 1996. **271**(33): p. 20208-12.

83. Fan, G., L.M. Ballou, and R.Z. Lin, *Phospholipase C-independent activation of glycogen synthase kinase-3beta and C-terminal Src kinase by Galphaq.* J Biol Chem, 2003. **278**(52): p. 52432-6.

84. Kozasa, T. and A.G. Gilman, *Purification of recombinant G proteins from Sf9 cells by hexahistidine tagging of associated subunits. Characterization of alpha 12 and inhibition of adenylyl cyclase by alpha z.* J Biol Chem, 1995. **270**(4): p. 1734-41.

85. Chidiac, P., V.S. Markin, and E.M. Ross, *Kinetic control of guanine nucleotide binding to soluble Galpha(q).* Biochem Pharmacol, 1999. **58**(1): p. 39-48.

86. Runnels, L.W. and S.F. Scarlata, *Determination of the affinities between heterotrimeric G protein subunits and their phospholipase C-beta effectors.* Biochemistry, 1999. **38**(5): p. 1488-96.

87. Ballou, L.M., et al., *Galphaq binds to p110alpha/p85alpha phosphoinositide 3-kinase and displaces Ras.* Biochem J, 2006. **394**(Pt 3): p. 557-62.

88. Pacold, M.E., et al., *Crystal structure and functional analysis of Ras binding to its effector phosphoinositide 3-kinase gamma.* Cell, 2000. **103**(6): p. 931-43.

89. Chan, T.O., et al., *Small GTPases and tyrosine kinases coregulate a molecular switch in the phosphoinositide 3-kinase regulatory subunit.* Cancer Cell, 2002. **1**(2): p. 181-91.

90. Stoyanov, B., et al., *Cloning and characterization of a G protein-activated human phosphoinositide-3 kinase.* Science, 1995. **269**(5224): p. 690-3.

91. Withers, D.J., et al., *Disruption of IRS-2 causes type 2 diabetes in mice.* Nature, 1998. **391**(6670): p. 900-4.

92. Ducluzeau, P.H., et al., *Regulation by insulin of gene expression in human skeletal muscle and adipose tissue. Evidence for specific defects in type 2 diabetes.* Diabetes, 2001. **50**(5): p. 1134-42.

93. Katome, T., et al., *Use of RNA interference-mediated gene silencing and adenoviral overexpression to elucidate the roles of AKT/protein kinase B isoforms in insulin actions.* J Biol Chem, 2003. **278**(30): p. 28312-23.

94. Matsumoto, M., et al., *Dual role of transcription factor FoxO1 in controlling hepatic insulin sensitivity and lipid metabolism.* J Clin Invest, 2006. **116**(9): p. 2464-72.

95. Fruman, D.A., et al., *Hypoglycaemia, liver necrosis and perinatal death in mice lacking all isoforms of phosphoinositide 3-kinase p85 alpha.* Nat Genet, 2000. **26**(3): p. 379-82.

96. Terauchi, Y., et al., *Increased insulin sensitivity and hypoglycaemia in mice lacking the p85 alpha subunit of phosphoinositide 3-kinase.* Nat Genet, 1999. **21**(2): p. 230-5.

97. Ueki, K., et al., *Increased insulin sensitivity in mice lacking p85beta subunit of phosphoinositide 3-kinase.* Proc Natl Acad Sci U S A, 2002. **99**(1): p. 419-24.

98. Bi, L., et al., *Early embryonic lethality in mice deficient in the p110beta catalytic subunit of PI 3-kinase.* Mamm Genome, 2002. **13**(3): p. 169-72.

99. Bi, L., et al., *Proliferative defect and embryonic lethality in mice homozygous for a deletion in the p110alpha subunit of phosphoinositide 3-kinase.* J Biol Chem, 1999. **274**(16): p. 10963-8.

100. Okkenhaug, K., et al., *Impaired B and T cell antigen receptor signaling in p110delta PI 3-kinase mutant mice.* Science, 2002. **297**(5583): p. 1031-4.

101. Foukas, L.C., et al., *Critical role for the p110alpha phosphoinositide-3-OH kinase in growth and metabolic regulation.* Nature, 2006. **441**(7091): p. 366-70.

102. Ciraolo, E., et al., *Phosphoinositide 3-kinase p110beta activity: key role in metabolism and mammary gland cancer but not development.* Sci Signal, 2008. **1**(36): p. ra3.

103. Martelli, A.M., et al., *Phosphatidylinositol 3-kinase translocates to the nucleus of osteoblast-like MC3T3-E1 cells in response to insulin-like growth factor I and platelet-derived growth factor but not to the proapoptotic cytokine tumor necrosis factor alpha.* J Bone Miner Res, 2000. **15**(9): p. 1716-30.

104. Gupta, S., et al., *Binding of ras to phosphoinositide 3-kinase p110alpha is required for ras-driven tumorigenesis in mice.* Cell, 2007. **129**(5): p. 957-68.

105. Lin, H.Y., L.M. Ballou, and R.Z. Lin, *Stimulation of the alpha1A adrenergic receptor inhibits PDGF-induced PDGF beta receptor Tyr751 phosphorylation and PI 3-kinase activation.* FEBS Lett, 2003. **540**(1-3): p. 106-10.

106. Batty, I.H., I.N. Fleming, and C.P. Downes, *Muscarinic-receptor-mediated inhibition of insulin-like growth factor-1 receptor-stimulated phosphoinositide 3-kinase signalling in 1321N1 astrocytoma cells.* Biochem J, 2004. **379**(Pt 3): p. 641-51.

107. Howes, A.L., et al., *Akt-mediated cardiomyocyte survival pathways are compromised by G alpha q-induced phosphoinositide 4,5-bisphosphate depletion.* J Biol Chem, 2003. **278**(41): p. 40343-51.

108. Hutson, N.J., et al., *Studies on the alpha-adrenergic activation of hepatic glucose output. I. Studies on the alpha-adrenergic activation of phosphorylase and gluconeogenesis and inactivation of glycogen synthase in isolated rat liver parenchymal cells.* J Biol Chem, 1976. **251**(17): p. 5200-8.

109. Thomas, A.P., A. Martin-Requero, and J.R. Williamson, *Interactions between insulin and alpha 1-adrenergic agents in the regulation of glycogen metabolism in isolated hepatocytes.* J Biol Chem, 1985. **260**(10): p. 5963-73.

110. Lu, Z., et al., *Galpha q inhibits cardiac L-type Ca2+ channels through phosphatidylinositol 3-kinase.* J Biol Chem, 2005. **280**(48): p. 40347-54.